NASA TECHNICAL NOTE

NASA TN D-8387

NASA TN D-8387

OPTIMAL REUSABLE-TUG AND EXPENDABLE-KICKSTAGE TRAJECTORIES FOR HIGH-ENERGY PLANETARY MISSIONS INCLUDING CORRECTION FOR NODAL PRECESSION

Janos Borsody

Lewis Research Center
Cleveland, Ohio 44135

NATIONAL AERONAUTICS AND SPACE ADMINISTRATION · WASHINGTON, D. C. · DECEMBER 1976

1 Report No	2 Government Accession No	3 Recipient's Catalog No
NASA TN D-8387		

4 Title and Subtitle	5 Report Date
OPTIMAL REUSABLE-TUG AND EXPENDABLE-KICKSTAGE TRAJECTORIES FOR HIGH-ENERGY PLANETARY MISSIONS INCLUDING CORRECTION FOR NODAL PRECESSION	December 1976
	6 Performing Organization Code

7 Author(s)	8 Performing Organization Report No
Janos Borsody	E-8844
	10 Work Unit No
	491-02

9 Performing Organization Name and Address	11 Contract or Grant No
Lewis Research Center National Aeronautics and Space Administration Cleveland, Ohio 44135	

12 Sponsoring Agency Name and Address	13 Type of Report and Period Covered
National Aeronautics and Space Administration Washington, D. C 20546	Technical Note
	14 Sponsoring Agency Code

15 Supplementary Notes

16 Abstract

Equations are derived by using branched trajectory optimization techniques and the Maximum Principle to maximize the payload capability of a reusable Tug/expendable kickstage vehicle configuration for planetary missions. The two stages and the payload are launched into a low Earth orbit by a single Space Shuttle (SS). The analysis includes correction for precession of the SS orbit. This correction is done by the Tug. The Tug propels the payload and the kickstage to an energy beyond Earth escape and returns within a specified time to the precessed SS orbit After separating from the Tug, the kickstage accelerates the payload to the required injection conditions. Planetary injection conditions are specified by the mission energy and a fixed declination and right ascension of the outgoing asymptote. The multipoint boundary value problem resulting from the analysis is solved by a Newton-Raphson iteration technique. Partial derivatives of the boundary conditions are obtained by perturbing the initial conditions one at a time, integrating the trajectory and adjoint equations, and observing the changes in boundary conditions. Maximum payload capability is derived for two typical mission energies. In addition, the variations of several mission and stage parameters are also examined.

17 Key Words (Suggested by Author(s))	18 Distribution Statement
Space flight; Space rendezvous; Space transportation; Space Tugs	Unclassified - unlimited STAR Category 15

19 Security Classif (of this report)	20 Security Classif (of this page)	21 No of Pages	22 Price*
Unclassified	Unclassified	47	$4 00

* For sale by the National Technical Information Service, Springfield, Virginia 22161

OPTIMAL REUSABLE-TUG AND EXPENDABLE-KICKSTAGE TRAJECTORIES FOR HIGH-ENERGY PLANETARY MISSIONS INCLUDING CORRECTION FOR NODAL PRECESSION

by Janos Borsody
Lewis Research Center

SUMMARY

Equations are derived by using branched trajectory optimization techniques and the Maximum Principle to design trajectories that maximize the payload capability of a reusable, Space Shuttle upper stage (Tug)/expendable kickstage configuration for planetary missions. The analysis takes into account the Space Shuttle (SS) orbit nodal precession. The Tug/kickstage trajectories are designed to correct for this nodal precession. Since the kickstage is expended after payload injection, all nodal correction maneuvers are done by the Tug. Planetary injection conditions that must be satisfied at kickstage burnout are defined in terms of the mission energy and the declination and right ascension of the outgoing asymptote.

The multipoint boundary value problem resulting from the mathematical analysis has been solved by using a Newton-Raphson iteration technique. Partial derivatives of the boundary conditions required by this technique are approximated by perturbing the initial conditions one at a time, integrating the equations of motion and the adjoint variational equations, and observing the changes in boundary conditions. The amount by which each initial condition is perturbed is arbitrary; however, in obtaining the sample case results, it was found that a 0.1 percent perturbation gave sufficiently accurate partial derivatives. Using these partial derivatives and the Newton-Raphson iterator led to a stable and uniform convergence.

Numerical results are presented for a reusable cryogenic Tug design based on current state-of-the-art technology and an expendable, space-storable, pressure-fed kickstage. Detailed analyses of these trajectories are presented for two mission energies. In addition, the effects of several mission and stage parameters on payload capability are also investigated.

Nominal mission characteristics used for the sample cases analyzed include a 185-kilometer circular departure and rendezvous orbit with an orbital inclination of 28.5°. The Tug is constrained to return to the Space Shuttle (SS) within 1 day. It is further assumed that the Tug corrects for all nodal precession of the SS orbit during the outbound burn and the retroburn.

A 10-minute coast time after the first Tug burn is included to allow for safe separation of the expendable kickstage and payload from the Tug. At the end of this coast phase, the kickstage ignites and accelerates the payload to the desired injection conditions.

Detailed performance analysis was done for two energies, one typical of a comet mission ($50\ km^2/sec^2$) and the other representing an outer planet mission ($100\ km^2/sec^2$), for declinations of the outgoing asymptote between -34° and $+34^{\circ}$. Ideal impulsive performance calculations are shown to be highly optimistic for this mission because large gravitational and thrust-to-weight losses are encountered during the flight. Payload loss to correct for nodal precession is small for both missions.

A parametric analysis of several stage and mission parameters was also performed for the outer planet mission. The major mission and Tug parameters that were perturbed include initial SS orbital inclination, total trip time, Tug/kickstage separation coast time, and Tug and kickstage engine thrust levels. These results show that payload is very sensitive to thrust level and kickstage separation coast time. Optimum total Tug trip time for this mission is approximately 26 hours; however, the payload penalty for trip times between 20 and 36 hours is quite small

For a declination range between -34° and $+34^{\circ}$, maximum performance is obtained for Tug departure-orbit inclinations of 28.5°. Higher declinations can be reached by increasing the SS orbital inclination with small payload penalty.

INTRODUCTION

At the present time the National Aeronautics and Space Administration (NASA) is developing a reusable Space Shuttle (SS). The SS will deliver many different payloads to low Earth orbit. For missions beyond SS capability, a propulsive stage (or stages) along with the payload will be delivered and deployed by the SS into a low Earth orbit, and the propulsive stage (or stages) will inject the payload to its final orbit. This propulsive stage configuration can be expendable, reusable, or a combination thereof.

Previous NASA studies indicate that a substantial cost savings can be realized by using a reusable orbital propulsive stage. For the numerical example used in this report, a conceptual orbital propulsion stage has been selected, which will be referred to throughout this report as the "Tug." The projected cost savings for the Tug are partly due to retrieval, refurbishment, and reuse of spacecraft and partly achieved through the reuse of expensive propulsive-stage hardware. For mission energies beyond reusable Tug capability, either the expensive Tug hardware must be expended or multistage orbital operations have to be considered.

Performance of a single-stage reusable Tug for low-energy, inner planet missions has been analyzed in reference 1. In the present report a method is presented to determine the maximum performance capability of a reusable Tug and an expendable kickstage for medium-energy (comet) and high-energy (outer planet) missions. This configuration could be attractive since, instead of expending an expensive piece of hardware (the reusable Tug), only a less-expensive kickstage is expended to do the mission. It will be assumed that the Tug, expendable kickstage, and payload are launched with a single SS flight. This assumes that the Tug propellant load is varied with payload and kickstage weight to remain within the SS lift capability of 29 484 kilograms.

Previous performance analyses of a reusable/expendable stage configuration have been largely limited to ideal impulsive computations, which assume infinite Tug and kickstage thrust. It has been further assumed in these studies that each burn occurs in low Earth orbit at an optimum point along the orbit. In reality, all burns have finite length (in some cases, several minutes), and some of the burns are performed far from Earth (depending on the trajectory constraints), which results in substantial gravitational losses. Some planar integrated performance data have been presented for multistage vehicle configurations in reference 2 without corrections for nodal precession. In the present report the effects of finite thrust level as well as nodal correction for the SS orbital precession are included in the analysis.

Nodal precession is caused by the Earth's oblateness and to a first-order approximation it is a function of orbital inclination, eccentricity, semilatus rectum, and the time spent in orbit. Since the duration of this mission (the time from Tug departure to return to the SS orbit) is of the order of 1 day, the selected SS orbit precesses approximately 8°. The Tug will have to correct for this nodal precession in order to return

to rendezvous with the SS. Nodal precessions of the Tug orbits are negligible because of the large semilatus rectum and eccentricity of these orbits. If nodal precession of the SS orbit is ignored as in reference 2, it can be shown that the Tug trajectories become planar and, furthermore, that the payload becomes independent of declination. This greatly simplifies the analysis and the solution of the two-point boundary value problem.

The purpose of the present report is twofold. One is to derive the equations that govern this complex mathematical optimization problem; the other is to apply the resulting equations to a sample case and to evaluate the effects of nodal change on payload and flight profile.

The mathematical equations are derived by using branched trajectory optimization techniques and the Maximum Principle. The multipoint boundary value problem resulting from this analysis is solved by using a Newton-Raphson iterator. Partial derivatives of the boundary conditions with respect to the free initial conditions required by this iterator are obtained from finite difference perturbations.

The method derived in this report was used to calculate the maximum payload capability for a fixed vehicle configuration and two mission energies of interest. The first energy (50 km^2/sec^2) is typical of a high-energy inner planet, comet, or asteroid mission; the second (100 km^2/sec^2) is a typical outer planet mission energy requirement.

The nominal vehicle selected for the sample case analysis consists of a cryogenic Tug and a space-storable kickstage. The Tug performance is based on a design that uses hydrogen and oxygen propellants; the pressure-fed, kickstage performance is based on a design that uses fluorinated oxygen and monomethyl hydrazine (MMH) propellants.

The effects of some trajectory parameters such as departure-orbit inclination, total trip time, and Tug/kickstage separation coast time on payload are investigated and discussed. The effect of Tug and kickstage thrust on payload is also investigated. These parametric studies were done only for the outer planet mission.

ANALYSIS

In the following sections the trajectory profiles are discussed in detail. Assumptions and constraints associated with the problem are presented, and the mathematical optimization problem is formulated in the framework of the Maximum Principle. From this formulation and the transversality conditions, a set of auxiliary variational conditions are derived. These variational conditions are further reduced to give a set of boundary conditions that must be satisfied in order to maximize payload. A short dis-

cussion of the procedure used to solve the two-point boundary value problem resulting from the analysis is also included.

Flight Profile and Simplifying Assumptions

A planar trajectory profile is presented in sketch (a) for the mission to be analyzed.

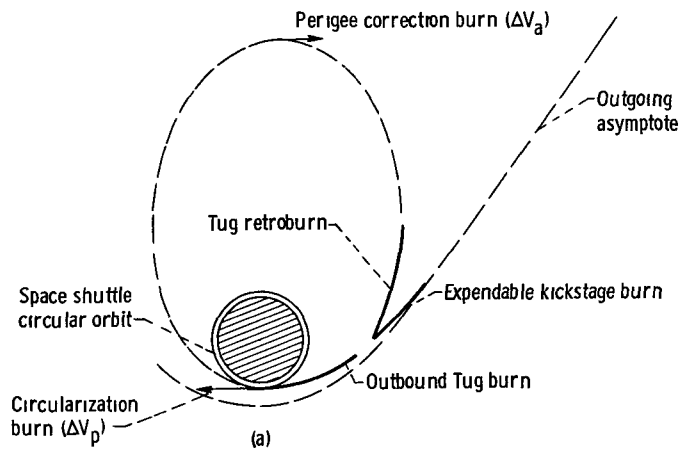

The flight profile consists of four burns by the Tug (outbound burn, retroburn, and apogee and perigee burns) and a single kickstage burn. The outbound Tug burn takes the kickstage and payload past Earth escape. This burn is followed by a fixed coast phase, which allows the Tug and kickstage to separate and the Tug to turn around to orient it for a retroburn. Retroburn is necessary because at separation the Tug is on an escape hyperbola and in order for it to return to the SS an elliptic return orbit must be established. Since during retroburn the Tug engine is pointed toward the kickstage and payload, plume impingement (causing possible payload contamination or damage to sensitive instrumentation) could be a problem. Also the highly corrosive exhaust products of the space-storable kickstage could damage the Tug, making refurbishment of this stage more difficult and costly. To alleviate this problem, a separation velocity must be imparted to the kickstage and payload, and the coast time must be kept long enough to allow for a safe separation distance to be achieved before either the Tug or the kickstage are ignited. The required separation distance for this configuration has not been established and a fixed coast time is assumed for this analysis. At the end of this coast phase the Tug performs the retroburn, while the kickstage accelerates the payload to its given planetary injection conditions. Retroburn is terminated primarily to satisfy a given trip time. The Tug is also constrained to be in the same orbital plane at retroburnout as the SS will be in at rendezvous. This constraint was introduced to correct for nodal precession of the SS orbit.

Nodal precession is caused by the Earth's oblateness, which induces a retrograde rotation of the SS orbit about the polar axis. This rotation is about 8 degrees per day for the selected SS orbit. Since the total Tug trip time (time from Tug departure from, to return to, the SS orbit) is about 1 day, the Tug must make an 8^{o} plane change during the outbound burn and the retroburn. The flight following the retroburn will be planar. At the apogee of the intermediate orbit, established at retroburnout, a small perigee correction burn is performed followed by a perigee burn to accomplish the rendezvous with the SS. These burns are assumed to be impulsive and to occur exactly at apogee and perigee in the analysis. Gravitational and thrust-to-weight losses should be very small for these two burns since the burns are short and the thrust-to-weight ratio is quite high.

The outbound burn, retroburn, and kickstage burn are numerically integrated, but the apogee and perigee burns are done impulsively. The assumption of impulsive apogee and perigee burns is made in order to simplify the mathematical optimization problem. It affects the problem in two ways: First, it allows these burns to be included analytically, which reduces by four the number of variational boundary conditions that must be satisfied. Second, the equations of motion and the adjoint variational equations must be integrated only to the end of the retroburn (a small fraction of the total Tug trip time). This greatly reduces the effects of roundoff errors and error propagation and consequently improves the accuracy of the finite-difference partial derivatives required by the Newton-Raphson iteration. The flight during the integrated burns is three dimensional and uses the optimum steering law.

The analysis presented herein assumes that all nodal correction is done during the outbound burn and the retroburn. An alternative to this approach would be to introduce an additional nodal correction burn, or some nodal correction could be done during the impulsive apogee and perigee burns. These approaches were not analyzed, and it is not clear if they offer any theoretical improvement over the approach used in this report. Based on the results obtained, the added nodal correction burn, even if theoretically optimum, may not be justified since the payload loss due to nodal correction is quite small as is shown in the RESULTS AND DISCUSSION section. Although small payload gains might be realized by the addition of a nodal correction burn, the losses associated with the additional startup and shutdown of a real engine could substantially reduce the expected payload gain.

In addition to these constraints the following assumptions were made in deriving the equations of motion governing the problem:

(1) A spherical nonrotating Earth model is assumed. This implies that there is no nodal or apsidal precession of the Tug orbits and that the Tug will correct for nodal precession of the SS orbit only. This gives a somewhat conservative vehicle performance since, if the Tug orbits were allowed to precess, the total nodal correction required would be slightly less and consequently the payload capability would be greater. For

the sample cases analyzed, nodal precession of the Tug orbits is less than 0.2° compared with a total SS-orbit nodal precession of approximately 8°.

(2) The right ascension of the outgoing asymptote is not constrained in the trajectory optimization. Instead an optimal "pseudo right ascension" is obtained for each declination of the outgoing asymptote. Pseudo right ascension is defined as the longitude of the projection of the outgoing asymptote in the equatorial plane measured from the ascending node of the initial SS orbit. The true right ascension, then, is the sum of the pseudo right ascension and the longitude of the SS-orbit ascending node as measured from the vernal equinox. The longitude of the SS-orbit ascending node is a function of the SS launch time and launch azimuth. For a fixed SS launch azimuth and a 1-day launch window the longitude of the SS-orbit ascending node sweeps through 360°, and any desired right ascension can be obtained simply by selecting the proper SS launch time.

(3) The reusable Tug and the expendable kickstage are assumed to have a constant engine exhaust velocity (specific impulse) and thrust, although the analysis is formulated to accommodate a variable thrust (and flow rate).

(4) The analysis is done for a two-body problem, and all perturbations due to the Sun, Moon, and planets are neglected.

(5) The Tug departs from and returns to a circular SS orbit. The longitude of the line of nodes of the initial SS orbit is fixed, and the Tug is free to depart at an optimum point along this orbit. The assumption of a circular SS orbit greatly simplifies the return-orbit geometry and rendezvous requirements. For elliptic SS orbits the line of apsides of the final Tug orbit must coincide with that of the precessed SS orbit, and additional constraints would have to be imposed on the problem. This apsidal constraint is discussed in more detail in the following section.

Nodal and Apsidal Precession

Nodal and apsidal precession were analyzed and analytic equations were derived in reference 3. For convenience they are reproduced here. Symbols and notation used in the following equations and the analysis are defined in appendix A.

$$\Delta\Omega = -\frac{J\sqrt{G}}{R_E^{3/2}} T_D \left(\frac{R_E}{p}\right)^{7/2} (1 - e^2)^{3/2} \cos i \qquad (1)$$

and

$$\Delta\omega = \frac{J\sqrt{G}}{2R_E^{3/2}} T_D \left(\frac{R_E}{p}\right)^{7/2} (1 - e^2)^{3/2} (4 - 5 \sin^2 i) \tag{2}$$

Nodal precession $\Delta\Omega$ and apsidal motion $\Delta\omega$ are functions of the inclination, eccentricity, and semilatus rectum of the particular orbit. They also depend on the total time T_D spent in orbit (total trip time). In equations (1) and (2), J, G, and R_E are the second harmonic in the gravitational potential function (oblateness parameter), the gravitational constant, and the equatorial radius of the Earth, respectively.

Equation (1) is used in the analysis to compute SS-orbit nodal precession. Note that the line of nodes moves at a constant rate in the retrograde direction for the given SS orbit.

Apsidal motion, given by equation (2), becomes an important consideration if elliptic SS orbits are used. For circular orbits the apsidal precession translates into an effective reduction in the period of the SS orbit. However, this can easily be taken care of with minor payload loss or gain by varying the total trip time a few minutes. Although theoretically proper phasing of Tug and SS can be achieved by varying total trip time, the operational aspects of this approach on Tug guidance hardware and software must be carefully evaluated. These requirements are outside the scope of this report and are not considered further.

Equations of Motion Governing the Problem

Based on the assumptions discussed in the previous sections equations of motion governing the problem are presented here. The variables and other notation used in this report are defined in appendix A. Equations governing the flight of a rocket in an inverse-square gravitational field are given by

$$\dot{\overline{V}} = -\frac{G}{r^2}\hat{r} + \frac{V_e \beta(\zeta)}{m}\hat{f} \tag{3}$$

$$\dot{\overline{r}} = \overline{V} \tag{4}$$

$$\dot{m} = -\beta(\zeta) \tag{5}$$

$$\dot{\zeta} = 1 \tag{6}$$

$$\hat{f} \cdot \hat{f} - 1 = 0 \tag{7}$$

In these equations V_e is the rocket exhaust velocity, β the mass flow rate as a function of time, and $\hat{f}$ the unit thrust direction. The superscripts $\bar{}$ and $\hat{}$ represent vector and unit vector quantities, respectively, and $\cdot$ denotes the time derivative of the particular variable. State variables r, V, m, and ζ are radius, velocity, mass, and a dummy variable associated with mass flow rate, respectively. By using a Hamiltonian formulation of the Maximum Principle, adjoint equations associated with the state variables can be obtained from the Hamiltonian given by

$$H = \bar{\lambda} \cdot \dot{\bar{V}} + \bar{\mu} \cdot \dot{\bar{r}} + \sigma \dot{m} + \tau \dot{\zeta} + \gamma(\hat{f} \cdot \hat{f} - 1) \tag{8}$$

The terms $\bar{\lambda}$, $\bar{\mu}$, σ, and τ in equation (8) are the adjoint variables associated with the state variables $\bar{V}$, $\bar{r}$, m, and ζ, respectively. The thrust magnitude constraint given by equation (7) is adjoined to H by γ.

From equation (8) the time derivatives of the adjoint variables on each trajectory phase are given by

$$\dot{\bar{\lambda}} = -\bar{\mu} \tag{9}$$

$$\dot{\bar{\mu}} = \frac{G}{r^3}\left[\bar{\lambda} - 3(\bar{\lambda} \cdot \hat{r})\hat{r}\right] \tag{10}$$

$$\dot{\sigma} = \frac{V_e \beta(\zeta)}{m^2}(\bar{\lambda} \cdot \hat{f}) \tag{11}$$

$$\dot{\tau} = -K \frac{\partial \beta(\zeta)}{\partial \zeta} \tag{12}$$

where

$$K = \frac{V_e}{m}(\bar{\lambda} \cdot \hat{f}) - \sigma \tag{13}$$

The thrust direction that minimizes equation (8) is given by

$$\hat{f} = \hat{\lambda} \tag{14}$$

and

$$\gamma = -\frac{V_e \beta \lambda}{2m} \tag{15}$$

To solve the multipoint boundary value problem determined by some initial, final, and intermediate boundary conditions, state equations (3) to (5) and adjoint equations (9) to (12) must be numerically integrated. Optimum thrust direction is along the unit λ vector given by equation (14).

Boundary Conditions and Constraints

In the following paragraphs, problem constraints and the mission profile are discussed in more detail. Sketch (b) illustrates the simplified trajectory profile with the

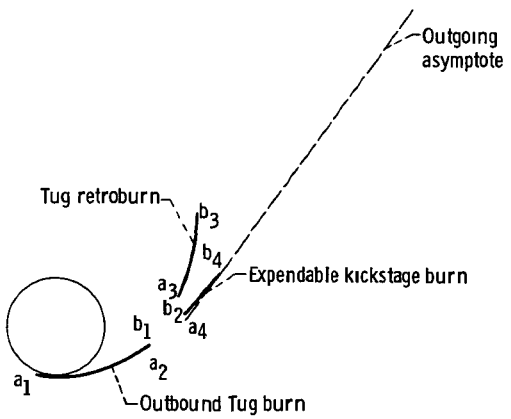

(b)

Tug and expendable kickstage departing from a given initial orbit. Outbound Tug burn is initiated at time $a_1 = 0$ at an optimum argument of latitude in the initial circular inclined orbit. Thrust is terminated at time b_1, followed by a fixed coast phase to time b_2. During the coast phase, the payload and kickstage (payload attached to the kickstage) are separated from the Tug. The Tug is turned around, and a safe separation distance is established for both kickstage firing and Tug retroburn firing. The Tug retroburn and the fixed kickstage burn start at times a_3 and a_4 ($a_3 = a_4 = b_2$), respectively. At kickstage burnout b_4 the desired energy and declination must be achieved. Tug retroburn is terminated upon reaching an orbit that will achieve the specified total trip time when followed by apogee and perigee delta velocity maneuvers. With these time conventions, the constraints governing the problem can be written mathematically as follows:

$$q_1 = r(a_1) - r_1 = 0 \tag{16.1}$$

$$q_2 = V(a_1) - V_1 = 0 \tag{16.2}$$

$$q_3 = \overline{r}(a_1) \cdot \overline{V}(a_1) = 0 \tag{16.3}$$

$$q_4 = \hat{h}(a_1) \cdot \hat{\imath}_3 - \cos i_1 = 0 \tag{16.4}$$

$$q_5 = -\hat{h}(a_1) \cdot \hat{\imath}_2 - \cos \Omega_1 \sin i_1 = 0 \tag{16.5}$$

$$q_6 = m(a_1) - m_1 = 0 \tag{16.6}$$

$$q_7 = \zeta(a_1) - a_1 = 0 \tag{16.7}$$

$$q_8 = a_1 = 0 \tag{16.8}$$

$$\overline{q}_9 = \overline{r}(a_2) - \overline{r}(b_1) = \overline{0} \tag{16.9}$$

$$\overline{q}_{10} = \overline{V}(a_2) - \overline{V}(b_1) = \overline{0} \tag{16.10}$$

$$q_{11} = m(a_2) - m(b_1) = 0 \tag{16.11}$$

$$q_{12} = \zeta(a_2) - \zeta(b_1) = 0 \tag{16.12}$$

$$\overline{q}_{13} = \overline{r}(a_3) - \overline{r}(b_2) = \overline{0} \tag{16.13}$$

$$\overline{q}_{14} = \overline{V}(a_3) - \overline{V}(b_2) = \overline{0} \tag{16.14}$$

$$q_{15} = m(a_3) + m(a_4) - m(b_2) = 0 \tag{16.15}$$

$$q_{16} = \zeta(a_3) - \zeta(b_2) = 0 \tag{16.16}$$

$$\overline{q}_{17} = \overline{r}(a_4) - \overline{r}(b_2) = \overline{0} \tag{16.17}$$

$$\overline{q}_{18} = \overline{V}(a_4) - \overline{V}(b_2) \doteq \overline{0} \tag{16.18}$$

$$q_{19} = \zeta(a_4) - \zeta(b_2) = 0 \tag{16.19}$$

$$q_{20} = a_2 + \Delta t - b_2 = 0 \tag{16.20}$$

$$q_{21} = \hat{r}(b_3) \cdot \hat{h}_o = 0 \tag{16.21}$$

$$q_{22} = \hat{V}(b_3) \cdot \hat{h}_o = 0 \tag{16.22}$$

$$q_{23} = m(b_3) - m_H e^{\Delta V_T / V_{e,1}} = 0 \tag{16.23}$$

$$q_{24} = b_3 - a_1 + T - T_D = 0 \tag{16.24}$$

$$q_{25} = E\left[r(b_4), V(b_4)\right] - E_D = 0 \tag{16.25}$$

$$q_{26} = \varphi\left[r(b_4), V(b_4)\right] - \varphi_D = 0 \tag{16.26}$$

$$q_{27} = m(a_4) - m(b_4) - m_{pk} = 0 \tag{16.27}$$

$$q_{28} = a_2 - b_1 = 0 \tag{16.28}$$

$$q_{29} = a_3 - b_2 = 0 \tag{16.29}$$

$$q_{30} = a_4 - b_2 = 0 \tag{16.30}$$

Equations (16.1) to (16.8) describe the given initial conditions at the beginning of outbound Tug burn. The only free orbital element is the argument of latitude where the burn starts, which will be used as an initial condition in solving the two-point boundary value problem. Equations (16.9) to (16.20) are constraints expressing the continuity of state variables at times a_2, a_3, and a_4. In equation (16.15), $m(a_4)$ is the combined kickstage and payload mass and, in equation (16.20), Δt is a fixed coast time. The Tug is constrained to return to a desired final orbit that coincides with the precessed SS orbit at rendezvous. This constraint is expressed by equations (16.21) and (16.22). Tug retroburn is terminated when the total-trip-time constraint (eq. (16.24)) is satisfied, and at this point the Tug must have sufficient propellant remaining for the ideal impulsive apogee and perigee maneuvers required to return the Tug to the SS (eq. (16.23)). The kickstage after a fixed burn (eq. (16.27)) must satisfy a desired energy (eq. (16.25))

and declination of the outgoing asymptote (eq. (16.26)). Equations (16.28) to (16.30) establish continuity in time at staging points along the trajectory. By using the theory of branched trajectory optimization (refs. 4 and 5) a set of variational boundary conditions are derived in the following paragraphs from the constraints previously described and an augmented Hamiltonian given by

$$H^* = -m(b_4) + \sum_{i=1}^{4} H_i + \sum_{i=1}^{30} \epsilon_i q_i$$

where $m(b_4)$ is the mass at kickstage burnout that will be maximized and H_i are the Hamiltonians during outbound burn, Tug/kickstage separation coast time, Tug retroburn, and kickstage burn. Constraints q_i are adjoined to H^* by using the arbitrary multipliers ϵ_i. Auxiliary variational conditions associated with the multipoint boundary value problem can be derived by using this augmented Hamiltonian.

Auxiliary Variational Equations

The constraints described in the previous section and the augmented Hamiltonian are used to satisfy the following auxiliary variational equations in order to maximize payload:

$$\bar{\lambda}(a_1) = \epsilon_2 \hat{V}(a_1) + \epsilon_3 \bar{r}(a_1) + \epsilon_4 \nabla_{\bar{V}} q_4 + \epsilon_5 \nabla_{\bar{V}} q_5 \tag{17.1}$$

$$\bar{\mu}(a_1) = \epsilon_1 \hat{r}(a_1) + \epsilon_3 \bar{V}(a_1) + \epsilon_4 \nabla_{\bar{r}} q_4 + \epsilon_5 \nabla_{\bar{r}} q_5 \tag{17.2}$$

$$\bar{\lambda}(a_2) = \bar{\lambda}(b_1) \tag{17.3}$$

$$\bar{\mu}(a_2) = \bar{\mu}(b_1) \tag{17.4}$$

$$\sigma(a_2) = \sigma(b_2) \tag{17.5}$$

$$\tau(a_2) = \tau(b_1) \tag{17.6}$$

$$\bar{\lambda}(a_3) + \bar{\lambda}(a_4) = \bar{\lambda}(b_2) \tag{17.7}$$

$$\bar{\mu}(a_3) + \bar{\mu}(a_4) = \bar{\mu}(b_2) \tag{17.8}$$

$$\sigma(a_3) = \sigma(b_2) \tag{17.9}$$

$$\tau(a_3) + \tau(a_4) = \tau(b_2) \tag{17.10}$$

$$\sigma(a_4) = \sigma(b_2) + \sigma(b_4) - 1 \tag{17.11}$$

$$\bar{\lambda}(b_3) + \frac{\epsilon_{22}}{V(b_3)} \hat{h}_o + \sigma(b_3) \frac{m(b_3)}{V_{e,1}} \nabla_{\bar{V}} \Delta V_T + H(b_3) \nabla_{\bar{V}} T = \bar{0} \tag{17.12}$$

$$\bar{\mu}(b_3) + \frac{\epsilon_{21}}{r(b_3)} \hat{h}_o + \sigma(b_3) \frac{m(b_3)}{V_{e,1}} \nabla_{\bar{r}} \Delta V_T + H(b_3) \nabla_{\bar{r}} T = \bar{0} \tag{17.13}$$

$$\tau(b_3) = 0 \tag{17.14}$$

$$\bar{\lambda}(b_4) + \epsilon_{25} \nabla_{\bar{V}} E + \epsilon_{26} \nabla_{\bar{V}} \varphi = \bar{0} \tag{17.15}$$

$$\bar{\mu}(b_4) + \epsilon_{25} \nabla_{\bar{r}} E + \epsilon_{26} \nabla_{\bar{r}} \varphi = \bar{0} \tag{17.16}$$

$$\tau(b_4) = 0 \tag{17.17}$$

$$H(b_4) = 0 \tag{17.18}$$

$$H(a_2) + H(a_3) + H(a_4) - H(b_1) - H(b_2) = 0 \tag{17.19}$$

In these equations, ϵ_i are arbitrary constants that must be evaluated to obtain the desired variational final conditions. Variational boundary conditions at the beginning of outbound Tug burn are given by equations (17.1) and (17.2). There are six of these equations and five arbitrary constants. Therefore, there is one variational condition that can be used as a final condition; it will be derived later. Equations (17.3) to (17.6) give the continuity of adjoint variables at the end of the outbound Tug burn; equations (17.7) to (17.11) give the conditions at the end of the Tug/kickstage separation coast phase. Variational conditions at retroburn completion are given by equations (17.12) to (17.14), and variational conditions at kickstage final burnout by equations (17.15) to (17.18). The Hamiltonian evaluated at various times along the trajectory must satisfy equation (17.19).

Gradients of return time T, total delta velocity ΔV_T, and declination φ with respect to $\bar{r}$ and $\bar{V}$ have been derived in reference 1 and will not be reproduced herein.

The variational auxiliary conditions given by equations (17) must be satisfied by the optimal trajectory in order to maximize payload. The arbitrary constants in these equations and the available variational boundary conditions are evaluated in the following sections. Conditions at the end of outbound Tug burn and at the start of Tug/kickstage separation coast phase can all be satisfied directly (eqs. (17.3) to (17.6)) by setting the corresponding variables at a_2 equal to those at b_1 and will not be discussed in more detail.

As has been mentioned, some of the auxiliary variational equations contain arbitrary constants that must be evaluated or eliminated from the equations to obtain the required variational boundary conditions. For example, there are six equations given by (17.1) and (17.2) with five arbitrary constants. The arbitrary constants could be evaluated from any combination of five of these equations. Once the constants are known, the resulting independent equation can be used as a free boundary condition. The form of this boundary condition will depend on the choice of equations used in computing the arbitrary constants. An alternative to computing these arbitrary constants is to find a function (a combination of two three-dimensional vector equations, such as (17.1) and (17.2), and the state conditions) that is not a function of these arbitrary constants and to use this as the variational boundary condition to be satisfied. This, of course, assumes an a priori knowledge of the function to be used. Such a function has been found and will be used to evaluate some of the variational boundary conditions. When the form of this function is not known, the arbitrary constants will be evaluated. And the variational boundary conditions will be computed in a convenient (not necessarily orthogonal) coordinate system to assure that the variational conditions are independent.

Variational Condition at Departure from Initial Orbit

As was mentioned previously, there are six independent variational equations (eqs. (17.1) and (17.2)) that must be satisfied at departure from the given initial SS orbit. This set of equations has five arbitrary constants, leaving one variational condition that is available as a boundary condition. The free variational condition can be derived as follows: Define

$$\bar{C}(t) = \bar{\lambda}(t) \times \bar{V}(t) + \bar{\mu}(t) \times \bar{r}(t) \tag{18}$$

where $\times$ represents the vector product of two vectors. From equations (17.1) and (17.2), the $\bar{C}$ vector at time a_1 is given by

$$\bar{C}(a_1) = \epsilon_4\left[\nabla_{\bar{V}} q_4 \times \bar{V}(a_1) + \nabla_{\bar{r}} q_4 \times r(a_1)\right] + \epsilon_5\left[\nabla_{\bar{V}} q_5 \times \bar{V}(a_1) + \nabla_{\bar{r}} q_5 \times \bar{r}(a_1)\right]$$

Substituting the gradients of q_4 and q_5 with respect to $\bar{V}(a_1)$ and $\bar{r}(a_1)$ into $\bar{C}(a_1)$ gives

$$\bar{C}(a_1) = (\epsilon_4 \hat{l}_3 - \epsilon_5 \hat{l}_2) \times \hat{h}(a_1) \tag{19}$$

Equation (19) implies that $\bar{C}(a_1)$ is perpendicular to $\hat{h}(a_1)$; consequently, their scalar product is zero, which is the required free variational condition

$$\bar{C}(a_1) \cdot \hat{h}(a_1) = 0 \tag{20}$$

It is shown in reference 6, that the free initial adjoint variables $\bar{\lambda}(a_1)$ and $\bar{\mu}(a_1)$ can be replaced by a set of physically more meaningful parameters; namely, pitch attitude ψ, pitch rate $\dot{\psi}$, yaw attitude δ, yaw rate $\dot{\delta}$, and magnitude of λ and $\dot{\lambda}$. The derivatives of λ can be computed from equation (20) as shown by the same reference.

Variational Conditions at Kickstage Burnout

In this section, variational conditions are derived at kickstage burnout. The arbitrary constants ϵ_{25} and ϵ_{26} in equations (17.15) and (17.16) can be evaluated as follows: Compute $\bar{C}(b_4)$ from equation (18), giving

$$\bar{C}(b_4) = -\epsilon_{26}\bar{y} \tag{21.1}$$

where

$$\bar{y} = \nabla_{\bar{V}}\varphi \times \bar{V}(b_4) + \nabla_{\bar{r}}\varphi \times \bar{r}(b_4) \tag{21.2}$$

The magnitude of vector y is equal to 1 (as can be shown by using eq. (B5)); and from equation (21.1), ϵ_{26} is given by

$$\epsilon_{26} = -\bar{C} \cdot \bar{y} \tag{22}$$

Vector $\bar{y}$ is perpendicular to $\hat{l}_3$ ($\hat{l}_3 = 0,0,1$) as shown in appendix B, and a free variational condition may be obtained from equation (21.1) by

$$\bar{C}(b_4) \cdot \hat{i}_3 = 0 \tag{23}$$

The constant ϵ_{25} can be chosen to satisfy the magnitude of equation (17.15); that is,

$$\epsilon_{25} = \pm \frac{|\bar{\lambda}(b_4) + \epsilon_{26} \nabla_V \varphi|}{V(b_4)} \tag{24}$$

The choice of sign is determined as follows: Suppose the declination is arbitrary (then $\epsilon_{26} = 0$). With this assumption after substituting ϵ_{25} and ϵ_{26} into equation (17.15), that equation becomes

$$\bar{\lambda}(b_4) = \mp \frac{\lambda(b_4)}{V(b_4)} \bar{V}(b_4)$$

But the thrust direction is along $\hat{\lambda}$ and, at kickstage burnout, energy must be added essentially along the velocity vector in order for a desired energy to be reached. This indicates that the minus sign should be used in equation (24).

Another free variational condition is obtained by substituting equations (17.15) and (17.16) into equation (8)

$$H(b_4) = -\epsilon_{26} \left[-\frac{G}{r^3(b_4)} \nabla_{\bar{V}} \varphi \cdot \bar{r}(b_4) + \nabla_{\bar{r}} \varphi \cdot \bar{V}(b_4) \right] + \beta(b_4) \left[\frac{V_{e,2} \lambda(b_4)}{m(b_4)} - \sigma(b_4) \right] + \tau(b_4)$$

However,

$$-\frac{G}{r^3(b_4)} \nabla_{\bar{V}} \varphi \cdot \bar{r}(b_4) + \nabla_{\bar{r}} \varphi \cdot \bar{V}(b_4) = \frac{d\varphi}{dt}$$

along a coast phase, but declination along a coast phase is constant and $d\varphi/dt = 0$, giving

$$H(b_4) = \beta(b_4) \left[\frac{V_{e,2} \lambda(b_4)}{m(b_4)} - \sigma(b_4) \right] + \tau(b_4)$$

Substituting equations (17.17) and (17.18) into this equation gives

$$\beta(b_4)\left[\frac{V_{e,2}\lambda(b_4)}{m(b_4)} - \sigma(b_4)\right] = 0$$

In this equation, $\beta(b_4) \neq 0$ since, in order to reach the desired energy, thrust must be on and therefore,

$$\sigma(b_4) = \frac{V_{e,2}\lambda(b_4)}{m(b_4)}$$

Substituting this equation and equations (17.17) and (17.18) into equation (8) at time b_4 gives the desired variational boundary condition

$$-\frac{G}{r^3(b_4)}\bar{\lambda}(b_4) \cdot \bar{r}(b_4) + \bar{\mu}(b_4) \cdot \bar{V}(b_4) = 0 \tag{25}$$

Two additional variational final conditions can be derived by taking the scalar product of equations (17.15) and (17.16) with $\hat{V}(b_4)$ and $\hat{r}(b_4)$, respectively, giving

$$\left[\bar{\lambda}(b_4) + \epsilon_{25}\bar{V}(b_4) + \epsilon_{26}\nabla_{\bar{V}}\varphi\right] \cdot \hat{V}(b_4) = 0 \tag{26.1}$$

$$\left[\bar{\mu}(b_4) + \epsilon_{25}\frac{G}{r^3(b_4)}\bar{r}(b_4) + \epsilon_{26}\nabla_{\bar{r}}\varphi\right] \cdot \hat{r}(b_4) = 0 \tag{26.2}$$

Thus, there are four variational conditions at b_4 that can be used to solve the two-point boundary value problem given by equations (23), (25), (26.1), and (26.2).

Variational Conditions at Tug Retroburnout

The six equations at retroburnout given by equations (17.12) and (17.13) have three unknowns, the two arbitrary constants $\epsilon_{21}, \epsilon_{22}$ and $\sigma(b_3)$. To determine the three variational conditions implicit in the six equations, these unknowns must be determined. The arbitrary constants ϵ_{21} and ϵ_{22} are evaluated from $\bar{C}(b_3)$, given by

$$\bar{C}(b_3) = -\hat{h}_o \times \left[\epsilon_{22}\hat{V}(b_3) + \epsilon_{21}\hat{r}(b_3)\right] \tag{27}$$

This equation was derived from the results of reference 7, where it is shown that $\nabla_{\bar{V}} X \times \bar{V} + \nabla_{\bar{r}} X \times \bar{r} = \bar{0}$ if $X = X[r, V, \bar{r} \cdot \bar{V}]$. Since total delta velocity ΔV_T and return time T are of this form, the corresponding vector products are zero. Equations (27) implies that $\bar{C}(b_3)$ is perpendicular to $\hat{h}_o$ and that their scalar product is zero. One free variational condition is given by

$$\bar{C}(b_3) \cdot \hat{h}_o = 0 \tag{28}$$

The constants ϵ_{21} and ϵ_{22} are evaluated by taking the scalar product of equation (27) with $\bar{r}(b_3)$ and $\bar{V}(b_3)$, giving

$$\epsilon_{21} = - \frac{\bar{\mu}(b_3) \cdot \hat{h}(b_3)}{\hat{h}_o \cdot \hat{h}(b_3)} r(b_3) \tag{29.1}$$

$$\epsilon_{22} = - \frac{\bar{\lambda}(b_3) \cdot \hat{h}(b_3)}{\hat{h}_o \cdot \hat{h}(b_3)} V(b_3) \tag{29.2}$$

The adjoint multiplier $\sigma(b_3)$ is evaluated by substituting equations (17.12) to (17.14) into equation (8):

$$H(b_3)\left[1 - \frac{G}{r^3(b_3)} \nabla_{\bar{V}} T \cdot \bar{r}(b_3) + \nabla_{\bar{r}} T \cdot \bar{V}(b_3)\right] = -\sigma(b_3) \frac{m(b_3)}{V_{e,1}}$$

$$\left[- \frac{G}{r^3(b_3)} \nabla_{\bar{V}} \Delta V_T \cdot \bar{r}(b_3) + \nabla_{\bar{r}} \Delta V_T \cdot \bar{V}(b_3)\right]$$

$$+ \beta(b_3)\left[\frac{V_{e,1} \lambda(b_3)}{m(b_3)} - \sigma(b_3)\right] \tag{30}$$

However,

$$- \frac{G}{r^3(b_3)} \nabla_{\bar{V}} T \cdot \bar{r}(b_3) + \nabla_{\bar{r}} T \cdot \bar{V}(b_3) = \frac{dT}{dt}$$

and

$$-\frac{G}{r^3(b_3)}\nabla_{\bar{V}}\Delta V_T\cdot\bar{r}(b_3)+\nabla_{\bar{r}}\Delta V_T\cdot\bar{V}(b_3)=\frac{d\,\Delta V_T}{dt}$$

These equations are valid on a coast phase. However, the change in return time is equal to the change in time along the coast arc but opposite in sign ($dT/dt = -1$), and the delta apogee and perigee velocities required to return the Tug remain constant along a coast arc ($d\,\Delta V_T/dt = 0$). Substituting these results into equation (30) gives

$$\beta(b_3)\left[\frac{V_{e,1}\lambda(b_3)}{m(b_3)}-\sigma(b_3)\right]=0$$

The mass flow rate $\beta(b_3)$ cannot be zero since thrusting must continue until a desired total trip time is reached at time b_3. Therefore

$$\sigma(b_3)=\frac{V_{e,1}\lambda(b_3)}{m(b_3)} \tag{31}$$

Two variational conditions can now be derived by taking the scalar product of equation (17.12) with $\nabla_{\bar{V}}\Delta V_T$ and the scalar product of equation (17.13) with $\nabla_{\bar{r}}\Delta V_T$ and substituting $\sigma(b_3)$, ϵ_{21}, and ϵ_{22}

$$\left[\bar{\lambda}(b_3)+\lambda(b_3)\nabla_{\bar{V}}\Delta V_T-\frac{\bar{\lambda}(b_3)\cdot\hat{h}(b_3)}{\hat{h}_o\cdot\hat{h}(b_3)}\hat{h}_o+H(b_3)\nabla_{\bar{V}}T\right]\cdot\nabla_{\bar{V}}\Delta V_T=0 \tag{32.1}$$

$$\left[\bar{\mu}(b_3)+\lambda(b_3)\nabla_{\bar{r}}\Delta V_T-\frac{\bar{\mu}(b_3)\cdot\hat{h}(b_3)}{\hat{h}_o\cdot\hat{h}(b_3)}\hat{h}_o+H(b_3)\nabla_{\bar{r}}T\right]\cdot\nabla_{\bar{r}}\Delta V_T=0 \tag{32.2}$$

where

$$H(b_3)=-\frac{G}{r^3(b_3)}\bar{\lambda}(b_3)\cdot\bar{r}(b_3)+\bar{\mu}(b_3)\cdot\bar{V}(b_3)$$

It is important that these derived variational conditions be independent, that is, that there exist no trivial solutions or that conditions previously derived do not already

satisfy these equations. It is easy to see that conditions (32.1) and (32.2) are independent by looking at the terms $\lambda(b_3)\left|\nabla_{\bar{V}}\,\Delta V_T\right|^2$ and $\lambda(b_3)\left|\nabla_{\bar{r}}\,\Delta V_T\right|^2$. These terms cannot be zero since the total delta velocity to return the Tug cannot be zero. The gradients cannot be zero since any change in radius and velocity will change ΔV_T. Also, the magnitude of $\lambda(b_3)$ is a function of these gradients and hence cannot be zero. Since these terms cannot be zero, a trivial solution cannot exist and the conditions are independent.

The three free variational boundary conditions derived herein are given by equations (28), (32.1), and (32.2)

Variational Conditions at Tug/Kickstage Separation

Equations (17.7), (17.18), and (17.10) express constraints that the adjoint variables must satisfy on an optimum trajectory. Adjoint variables $\bar{\lambda}$ and $\bar{\mu}$ are known at time b_2 (they are integrated from time a_1). If these variables were known at time a_3, the preceding equations could be used to compute them at a_4. At time a_3, $\bar{\lambda}$ and $\bar{\mu}$ are arbitrary; therefore, $\psi(a_3)$, $\dot{\psi}(a_3)$, $\delta(a_3)$, $\dot{\delta}(a_3)$, $\lambda(a_3)$, and $\dot{\lambda}(a_3)$ can be used as initial conditions to compute $\bar{\lambda}(a_3)$ and $\bar{\mu}(a_3)$. The derivative $\dot{\lambda}(a_3)$ is computed from equation (28) by using the procedure given in reference 6. The adjoint variable $\lambda(a_3)$ can also be computed as follows: From equations (17.7) and (17.8) the relation between the C vectors at kickstage separation is given by

$$\bar{C}(a_3) + \bar{C}(a_4) = \bar{C}(b_2) \tag{33}$$

The vector C is a constant of motion on every subarc ($\dot{\bar{C}}$ = constant). This can be verified by taking the time derivative of $\bar{C}$. After substituting for $\dot{\bar{\lambda}}$, $\dot{\bar{\mu}}$, $\dot{\bar{r}}$, and $\dot{\bar{V}}$, the time derivative $\dot{\bar{C}}$ becomes identically zero, which implies that $\bar{C}$ is a constant. Since $\bar{C}$ is a constant, $\bar{C}(a_4) = \bar{C}(b_4)$. Therefore, taking the scalar product of this equation with $\hat{\imath}_3$ and substituting equation (23) give $\bar{C}(a_4) \cdot \hat{\imath}_3 = 0$, and $\lambda(a_3)$ can be computed from equation (33) as

$$\lambda(a_3) = \frac{\bar{C}(b_2) \cdot \hat{\imath}_3}{\left[\dfrac{\bar{C}(a_3)}{\lambda(a_3)}\right] \cdot \hat{\imath}_3} \tag{34}$$

where

$$\left[\frac{\overline{C}(a_3)}{\lambda(a_3)}\right] = \hat{\lambda}(a_3) \times \hat{V}(a_3) - \frac{\left[\hat{\lambda}(a_3) \times \overline{V}(a_3) - \dot{\hat{\lambda}}(a_3) \times \overline{r}(a_3)\right] \cdot \hat{h}_o}{\left[\hat{\lambda}(a_3) \times \overline{r}(a_3)\right] \cdot \hat{h}_o} \left[\hat{\lambda}(a_3) \times \overline{V}(a_3) + \dot{\hat{\lambda}}(a_3) \times \overline{r}(a_3)\right]$$

the vectors $\hat{\lambda}(a_3)$ and $\dot{\hat{\lambda}}(a_3)$ are evaluated as shown in reference 6. Therefore, equation (34) can be used to compute the magnitude of λ at a_3.

Another variational final condition can be derived from equation (17.19).

$$H(a_2) + H(a_3) + H(a_4) - H(b_1) - H(b_2) = 0$$

Since H is constant on every branch,

$$H(a_2) = H(b_2)$$

And from equations (17.3) and (17.4)

$$-\frac{G}{r^3(b_2)} \cdot \overline{r}(b_2) + \overline{\mu}(b_2) \cdot \overline{V}(b_2) = -\frac{G}{r^3(b_1)} \overline{\lambda}(b_1) \cdot \overline{r}(b_1) + \overline{\mu}(b_1) \cdot \overline{V}(b_1)$$

Also from equation (17.18) and the constancy of H

$$H(a_4) = H(b_4) = 0$$

Substituting these results gives

$$H(a_3) = H(b_1) \tag{35}$$

From equation (11) it is obvious that σ is constant on a coast phase, and from equations (17.5) and (17.9)

$$\sigma(a_3) = \sigma(b_1)$$

Without loss of generality, assume $\beta(b_1) = \beta(a_3)$. Substituting these results and equation (17.10) into equation (35) gives

$$-\frac{G}{r^3(a_4)} \overline{\lambda}(a_4) \cdot \overline{r}(a_4) + \overline{V}(a_4) \cdot \overline{\mu}(a_4) + \tau(a_4) + V_{e,1}\beta(b_1)\left[\frac{\lambda(b_1)}{m(b_1)} - \frac{\lambda(a_3)}{m(a_3)}\right] \tag{36}$$

If the kickstage flow rate is constant, the adjoint variable τ also remains constant during the burn, and from equation (17.17) $\tau(a_4) = 0$. If the kickstage flow rate is variable, $\tau(a_4)$ is computed from

$$\tau(a_4) = \int_{a_4}^{b_4} K \frac{\partial \beta}{\partial t} dt \tag{37}$$

Initial and Final Conditions

Some of the initial conditions have been discussed in previous sections. In this section a complete set of initial and associated final conditions are given:

Initial conditions	Final conditions	
$\psi(a_1)$	$\hat{r}(b_3) \cdot \hat{h}_o = 0$	(38.1)
$\dot{\psi}(a_1)$	$\hat{V}(b_3) \cdot \hat{h}_o = 0$	(38.2)
$\delta(a_1)$	Equation (26.1)	(38.3)
$\dot{\delta}(a_1)$	Equation (26.2)	(38.4)
$\lambda(a_1)$	Equation (17.11)	(38.5)
$\dot{\lambda}(a_1)$	Equation (20)	(38.6)
b_1	$m(a_4) - m(b_4) - m_{pk} = 0$	(38.7)
$\psi(a_3)$	$\varphi(a_4) - \varphi_D = 0$	(38.8)
$\dot{\psi}(a_3)$	Equation (25)	(38.9)
$\delta(a_3)$	Equation (32.1)	(38.10)
$\dot{\delta}(a_3)$	Equation (32.2)	(38.11)
$\lambda(a_3)$	Equation (23)	(38.12)

$\dot{\lambda}(a_3)$	Equation (28)	(38.13)
b_3	$b_3 - a_1 + T - T_D = 0$	(38.14)
b_4	$E(b_4) - E_D = 0$	(38.15)
$m(a_3)$	$m(b_3) - m_h e^{\Delta V_T / V_{e,1}} = 0$	(38.16)
$u(a_1)$	Equation (36)	(38.17)

In solving the two-point boundary value problem, the 17 initial conditions must be guessed at and a numerical iteration process performed until the given final conditions are satisfied. The iteration size can be reduced to an 11-by-11 iteration as follows: Terminate the Tug retroburn and the kickstage burn when equations (38.15) and (38.14) are satisfied, respectively. Furthermore, equations (38.6), (38.12), and (38.13) can be used to compute $\dot{\lambda}(a_1)$, $\lambda(a_3)$, and $\dot{\lambda}(a_3)$, respectively; and final condition (38.5) can be satisfied trivially by scaling the problem with $\lambda(a_1)$.

The numerical results presented were obtained by using a Newton-Raphson iteration technique. Each initial condition was perturbed individually and the changes in final conditions observed in order to evaluate the partial derivatives of the final conditions with respect to the given initial conditions. The perturbation sizes of the initial conditions were determined empirically. Through trial and error it was determined that 0.1 percent perturbation of the initial conditions gave sufficiently accurate partial derivatives. Using these partials showed convergence for the sample cases to be well behaved and uniform. Some convergence difficulties were encountered for declinations whose absolute value exceeded initial SS orbital inclination. For these cases, payload decreases very rapidly with increasing declination of the outgoing asymptote, and the finite-difference partial derivatives become very sensitive to initial conditions. The numerical iteration process was continued until the expected percentage of payload improvement and the normalized final conditions were within a given tolerance.

RESULTS AND DISCUSSION

The method and equations developed in the earlier sections were applied to a given vehicle configuration and a range of planetary target conditions. The results of this analysis are presented in this section.

Nominal mission constraints and planetary injection conditions used in the sample case analysis are given in table I. As is discussed in the INTRODUCTION, a single-

stage Tug in the reusable mode can only be used for relatively low-energy missions. To extend the energy range of this reusable Tug to the region covering comet and outer planet missions an expendable kickstage was introduced. The reusable Tug delivers the kickstage and payload to some energy beyond Earth escape, and the kickstage provides the additional energy required for the mission. The energy range considered for the baseline vehicle configuration is from a vis-viva energy of 35 to 120 km^2/sec^2. The low end of the energy range is determined by the performance of the single-stage reusable Tug. At the high end the payload capability of the present configuration approaches zero. Departure-orbit altitude and inclination were chosen to be 185 kilometers and 28.5^o, respectively. This represents a due-east SS launch from the Eastern Test Range. Based on previous experience with single-stage reusable Tug trajectories (ref. 1), the total trip time was chosen to be 1 day and Tug/kickstage separation coast time was selected as 10 minutes. Although the 1-day trip time is nearly optimum for performance, the selection of 10-minute separation time was arbitrary, and significant payload gain can be realized if this time can be shortened.

In the analysis it is assumed that the Tug, kickstage, and payload are launched with a single SS. This assumption implies that the weight of the selected configuration is fixed (28 622 kg) and consistent with SS payload capability. To keep the initial weight fixed, the Tug propellant must be varied to accommodate changes in payload capability.

Baseline Tug characteristics are given in table II. Engine performance corresponds to that of an uprated RL-10 with a specific impulse of 460 seconds and an engine thrust of 66 723 newtons. The RL-10 engine is currently in use on the Centaur stage.

The characteristics of the space-storable kickstage were taken from reference 8 and are given in table III. The kickstage is pressure fed and has a specific impulse of 378 seconds. Because of its low thrust level (13 345 N) and the spatial location of this burn, the kickstage can be expected to have large gravitational losses.

As a first step in this study the range of useful payload was determined for this vehicle configuration. Maximum payload capability is determined as a function of mission energy for a 0^o declination. Selection of this declination is arbitrary, and it is intended to establish the useful payload range of this vehicle configuration as a function of mission energy. These results are presented in figure 1. For comparison, ideal impulsive payload capability without nodal correction is also given. Ideal impulsive performance was computed by assuming an infinite thrust for the Tug and kickstage and that all velocity change maneuvers would take place instantaneously at the same low altitude. Ideal, impulsive, mission delta velocities were computed based on the given mission energy. All velocity changes were assumed to be planar, and they do not account for plane change requirements due to nodal precision or changes in inclination to meet mission declination requirements. Note the large payload losses. At an energy of 100 km^2/sec^2 the ideal payload is 1200 kilograms and the loss due to gravitational and thrust-to-weight effects, nodal precession, etc., is 520 kilograms. Obviously,

ideal impulsive performance calculations for this configuration and mission are inadequate, and the trajectories must be integrated to include actual trajectory losses. To further analyze the behavior of these trajectories, two energies were selected: an energy of 50 km^2/sec^2, which corresponds to a high-energy inner planet or comet mission, and an energy of 100 km^2/sec^2, which corresponds to an outer planet mission.

To explain the results that follow, it is helpful to recall some facts from orbital geometry and previous analyses of planetary missions (ref. 1). If the SS-orbital nodal precession is assumed to be zero and a spherical Earth model is used, for a fixed SS orbit the same payload can be delivered, using planar trajectories, to all declinations of the outgoing asymptote (DLA) whose absolute value is less than the initial SS orbital inclination without using yawed trajectories. Furthermore, there are two distinct solutions for each DLA whose absolute value is less than the SS orbital inclination. As the DLA approaches the SS orbital inclination the two solutions approach one another, and at a DLA equal to the SS orbital inclination they degenerate into a single solution. Those DLA's whose absolute value is greater than the initial SS orbital inclination can be reached only if the Tug orbital inclination is increased to or beyond the absolute value of the desired DLA. To change orbital inclination at low-Earth-orbit altitudes is very costly, therefore, maximum performance for these DLA's is obtained when the orbital inclination is made equal to the absolute value of the desired DLA.

Another important point to recall is that, for a fixed out-of-plane acceleration, maximum change in the line of nodes is obtained when the out-of-plane acceleration is applied at the antinode and maximum change in orbital inclination is obtained when the yaw maneuver is done at the line of nodes (at the equator). An out-of-plane acceleration, which tends to increase inclination near the line of nodes, will move the line of nodes retrograde when applied before the nodal crossing and posigrade when applied after the nodal crossing. Obviously, since the line of nodes of the Tug orbits must be moved in a retrograde direction, inclination changes that move the node in this direction are desirable. An inclination change that moves the node posigrade is undesirable because it increases the total nodal correction that must be made later.

Based on equation (1) and nominal trajectory and mission parameters, the SS orbital precession is approximately 8° in a retrograde direction. The Tug will have to correct for this nodal precession during outbound burn and retroburn. Since the plane change maneuvers during Tug outbound burn and retroburn are small, the basic trajectory profiles are not expected to be drastically different from the planar trajectory profile without nodal correction. And the general conclusions drawn from the planar case are expected to apply to the more complex nonplanar trajectories.

Existence of the two distinct solutions for DLA's whose absolute value is less than the SS orbital inclination was shown numerically for the present problem. This was done by taking a converged case for a given DLA, changing the signs on initial yaw altitudes and rates, and adding 180° to the Tug departure argument of latitude. With these

initial conditions the trajectory was integrated and without any iteration gave a converged case for a DLA of the same magnitude but opposite sign. Both solutions will be presented for the two mission energies, although for simplicity the discussion will be restricted to one of the solutions. To eliminate confusion, results obtained from the second solution are shown by a dotted line in figures 2 to 13. Discussion of the results will be restricted to the first solution (solid line), but similar reasoning can be applied to the second solution.

Data presented in figures 2 to 7 as a function of the declination of the outgoing asymptote are for the 50-km^2/sec^2 energy case. Figure 2 gives the optimum pseudo right ascension. As was discussed earlier (in the section Flight Profile and Simplifying Assumptions), specific requirements on the right ascension of the outgoing asymptote can be satisfied for a given optimal pseudo right ascension by selecting the proper SS launch time. By subtracting the value of pseudo right ascension for the desired DLA from the required right ascension, the longitude of the ascending node for the SS orbit may be determined. Since the SS orbital longitude of the ascending node sweeps through 360^o for a fixed SS launch azimuth and a 1-day launch window, any desired right ascension of the outgoing asymptote may be obtained by selecting the proper SS launch time.

The point of Tug departure from the initial orbit was optimized and the results are presented as a function of DLA in figure 3. Departure argument of latitude is defined as the angle measured in the initial SS orbital plane from the ascending node of this orbit to the point where the outbound burn starts. Note the similarities between this and the previous figure. To explain the similar behavior of these figures from orbital geometry, recall that the shape of the escape hyperbola depends primarily on perigee radius (which changes little with DLA) and mission energy (which is constant). Therefore, once the trajectory is optimized for a given DLA, the shape of the escape hyperbola does not change significantly as DLA is varied. As DLA is changed, the plane of the escape hyperbola is essentially rotated about the angular momentum vector of the initial SS orbit until the desired DLA is satisfied. Therefore, as departure argument of latitude decreases so must pseudo right ascension.

Orbital inclination at Tug/kickstage separation and nodal correction during outbound Tug burn are presented in figures 4 and 5, respectively. To explain the trajectory characteristics obtained, recall the earlier discussion on the effect of out-of-plane maneuvers on the orbital inclination and the line of nodes. For negative DLA's whose absolute value is less than the SS orbital inclination the outbound burn starts past the line of nodes (fig. 3, solid line) and continues through a burn arc of approximately 100^o. Thus, a major protion of the outbound burn occurs near the antinode, which is an optimal region for changing the longitude of the line of nodes. Almost all the required nodal change (8^o) is done during this burn, as seen in figure 5. For negative DLA's whose absolute value is larger than the SS orbital inclination the orbital inclination must be increased to reach the desired DLA, as seen in figure 4. Orbital inclination at the

completion of the outbound Tug burn is less than the absolute value of the corresponding DLA. Since final spacecraft orbital inclination must be equal to the absolute value of the DLA, as was discussed earlier, the remaining inclination change is done during the kickstage burn. Note that nodal change during the outbound burn decreases as the absolute value of the DLA is increased beyond the SS orbital inclination. This is caused by the large inclination change being made during the outbound burn. Since the Tug must return to the SS orbit, the same inclination change must be made during retroburn, and it becomes more efficient to perform a larger nodal correction during this burn.

As the value of the DLA is increased from negative values to zero, the departure argument of latitude moves closer to the line of nodes and it becomes more difficult to make large nodal corrections during the outbound burn (fig. 5). Also for these DLA's the burn takes place past the line of nodes and orbital inclination must be decreased to move the node retrograde, as seen in figure 4. For DLA's between 10° and 20° the outbound burn traverses the line of nodes and nodal change for these cases is a minimum, as expected. As the DLA is further increased the outbound burn begins well before the nodal crossing and the nodal correction increases. Also orbital inclination increases to move the node retrograde. For DLA's larger than the SS orbital inclination a large inclination change is being made during the retroburn, and again it becomes more efficient to make larger nodal corrections during this burn. Consequently, nodal correction during outbound burn (fig. 5) decreases. Note the single solutions for high negative and positive DLA's. The reason these curves do not leave the closed curve exactly at DLA's equal to the SS orbital inclination is that orbital inclination must be changed during the outbound burn to correct for nodal precession.

Payload as a function of DLA is given on figure 6. Payload is maximum for DLA's of approximately $\pm 12^{\circ}$, and it varies less than 1 percent for DLA's between -28.5° and $+28.5^{\circ}$. Payload outside this range decreases rapidly because of the large inclination changes being made. Note that payloads for the two solutions are very close although the trajectory profiles are different. This is a result of the trade-off between losses during outbound burn and retroburn.

Velocity losses during the three main trajectory phases (outbound Tug burn, return leg (inbound), and kickstage burn) are given in figure 7. Velocity loss is defined as the velocity increment supplied by the vehicle (computed from the ideal rocket equation and the amount of propellant used by the vehicle) above the ideal impulsive velocity (as defined earlier) required to perform the mission. By this definition, the velocity loss during kickstage burn is large but remains nearly constant until the absolute value of the desired DLA exceeds the SS orbital inclination. A major portion of this velocity loss is caused by the trajectory constraints. The outbound Tug burn puts the kickstage and payload on an escape hyperbola. During this burn and the long coast phase that follows, the altitude increases very rapidly and the kickstage burn occurs at high altitudes, resulting in large losses. For DLA's whose absolute value is larger than the SS orbital

inclination, some inclination change is made during the kickstage burn and the losses increase rapidly. It should be pointed out that the velocity added to change orbital inclination in order to meet mission DLA requirements is not a loss. However, because of the definition of ideal impulsive mission velocity (which is independent of the DLA), the velocity required to change orbital inclination is included in the velocity losses along with the loss due to gravity and other trajectory-shaping losses. Outbound and inbound losses vary with DLA; however, the sum of these losses remains nearly constant. The trade-off between outbound and inbound velocity losses for the two solutions is obvious from this figure.

The same data discussed in the preceding paragraphs for an energy of 50 km^2/sec^2 are presented in figures 8 to 13 for an energy of 100 km^2/sec^2. Behavior of the data is very similar and will not be discussed in detail. Again the payload loss for a range of DLA's between -28.5^o and $+28.5^o$ is small, less than 1 percent of payload.

The data presented in figures 14 to 17 were derived for an outer planet mission. They show the effect on payload of variations in selected mission, Tug, and kickstage parameters. Since the payload curve is symmetric about 0^o DLA, the data presented are restricted to the solution giving maximum payload and positive DLA's. Data are provided for DLA's of 0^o, 10^o, 20^o, and 30^o.

Figure 14 shows the variation of payload with SS orbital inclination. All payload curves have a minimum at an initial orbital inclination of about 45^o. Since at an inclination of 90^o the nodal shift is zero, the optimum flight profile is planar. Payload loss due to nodal shift then is the difference between the payload at a given inclination and the payload for the 90^o inclination planar case. Maximum payload loss due to nodal shift for the sample mission (28.5^o orbital inclination, 30^o DLA, and 100-km^2/sec^2 mission energy) is 14 kilograms, or about 2.2 percent of the payload. Also, since the nodal correction for the 90^o initial SS orbital inclination is zero, the Tug payload capability is maximum for this case. However, the SS is limited by range-safety launch azimuth constraints to a maximum orbital inclination of 56^o for launch from the Eastern Test Range. The results presented in figure 14 were derived by assuming that the SS payload capability is constant and independent of orbital inclination. In the actual case, SS payload capability decreases as orbital inclination is increased, which would tend to reduce the indicated Tug/kickstage payload. Therefore, for initial SS orbital inclinations between 28.5^o and 56^o, maximum performance (for DLA's between -28^o and $+28^o$) is obtained by departing from a 28.5^o inclined orbit.

Data presented in figure 15 were obtained by varying the Tug/kickstage separation coast time. Payload capability is quite sensitive to this coast time. As coast time is increased from 2 minutes to 14 minutes, payload decreases from about 850 kilograms to 610 kilograms. This payload loss is caused by increased gravitational losses as coast time increases. Theoretically, optimal location for any burn is near perigee. At separation the Tug and kickstage are on an escape hyperbola. As coast time increases,

the two burns (retroburn and kickstage burn) will occur further and further from perigee. This, of course, increases gravitational losses and decreases payload.

Another important mission parameter that affects payload is total trip time. Total trip time is defined as the time from Tug departure to return to the SS orbit. For short trip times the nodal correction is small, but the losses during Tug retroburn become large; for long trip times the nodal correction becomes large and the losses during retroburn become small. Therefore, there is an optimal trip time that gives maximum payload. Payload as a function of trip time is presented in figure 16. Optimum trip time for this energy (100 km^2/sec^2) is approximately 26 hours. However, the payload penalty for trip times between 20 and 36 hours is quite small (less than 1 percent of the payload).

Another Tug parameter investigated is the Tug thrust level, and the effect on payload is presented in figure 17. As initial thrust increases, the payload capability also increases because of decreased gravitational losses. These data are obtained by assuming a constant Tug engine weight. In the actual case, engine weight varies with thrust, which will affect the indicated payload capability. To select an optimum thrust level for the Tug, the variation of engine weight with thrust level would have to be included in determining payload capability.

Kickstage burn (similar to the Tug retroburn) occurs on an escape hyperbola at high attitudes, and gravitational losses are large. These losses can be reduced by decreasing the kickstage burn time, which is equivalent to increasing the engine thrust level. The increase in payload capability that results from an increase in kickstage thrust is shown in figure 18. The results were obtained by assuming that the kickstage engine weight remains constant as its thrust varies. (The same assumption was made about Tug engine weight in determining the effect of Tug thrust on payload, as discussed previously.) In this case, however, there is a one-to-one trade-off between engine weight and payload weight, and actual payload capability can be computed by subtracting the change in engine weight for a given thrust from the indicated payload capability. Optimum kickstage thrust level could be determined from this type of figure for a given mission by including the effect of engine weight on payload.

SUMMARY OF RESULTS

In this report, mathematical equations were developed to obtain the maximum payload capability for a two-stage, Space Shuttle (SS) upper-stage configuration. This configuration consists of a reusable Tug and an expendable kickstage. The analysis assumes that correction for SS-orbit nodal precession is done by the Tug during the outbound burn and the retroburn. Planetary injection conditions are satisfied by a given energy and a given declination of the outgoing asymptote. The procedure presented may

be used to determine SS launch time to satisfy specific right ascension requirements for a given mission. The multipoint boundary value problem derived is solved by using a Newton-Raphson iterator. Partial derivatives required by this iteration technique are approximated by means of finite-difference techniques.

To demonstrate the capability of the analytic technique, these equations were applied to a vehicle configuration consisting of a cryogenic reusable Tug and a space-storable, pressure-fed, expendable kickstage.

Payload as a function of the declination of the outgoing asymptote was computed for mission energies of 50 and 100 km^2/sec^2 and a set of nominal mission constraints. For these nominal mission constraints the maximum payload capabilities for the two mission energies were 2400 and 680 kilograms, respectively. This represents payload losses of 820 and 520 kilograms, respectively, when compared with the payload capability determined by using ideal impulsive computations without nodal correction. Therefore, it is obvious that ideal impulsive payload computations are inadequate and that the trajectories must be integrated.

Perturbation analysis done for the outer-planet mission (vis-viva energy of 100 km^2/sec^2) shows that payload is quite sensitive to Tug thrust as well as to kickstage thrust and Tug/kickstage separation coast time. Optimum total trip time is approximately 26 hours; however, the payload loss for total trip times between 20 and 36 hours is quite small. Examination of departure-orbit inclination shows that maximum payload for an Eastern Test Range SS launch is obtained by departing from a 28.5° inclined orbit. Of course, when high declinations are required, the departure-orbit inclination must be increased.

The payload loss to correct for nodal precession is small (14 kg) for the optimal trajectories derived. The results further show that the energy range of a reusable Tug can be greatly extended by using this two-stage configuration and that significant payload capability is available for comet and asteroid types of missions and for some outer planet missions.

Lewis Research Center,
National Aeronautics and Space Administration,
Cleveland, Ohio, August 27, 1976,
491-02.

APPENDIX A

SYMBOLS

a	time at beginning of a phase, sec
b	time at end of a phase, sec
$\bar{C}$	defined by eq. (18), kg-sec
E	energy, m^2/sec^2
e	eccentricity
$\hat{f}$	unit thrust direction
G	gravitational constant of Earth, m^3/sec^2
H	Hamiltonian, kg
H^*	augmented Hamiltonian, kg
h	angular momentum, m^2/sec
$\hat{h}_o$	unit angular momentum vector of the return orbit
ı	inclination, rad
J	oblateness parameter (1.624×10^{-3})
K	kappa function defined by eq. (13), sec
l	right-handed Cartesian coordinate directions ($\hat{l}_1$ points to initial SS orbital line of nodes and $\hat{l}_3$ to North Pole)
m	mass, $kg\text{-}sec^2/m$
m_{pk}	kickstage propellant loading, kg
p	semilatus rectum, m
q	constraints
R_E	equatorial radius of Earth (6.37816×10^6 m)
r	radius, m
T	return time, sec
T_D	trip time, sec
t	time, sec
Δt	Tug/kickstage separation coast time, sec
V	velocity, m/sec

V_e exhaust velocity, m/sec

$V_{e,1}$ Tug exhaust velocity, m/sec

$V_{e,2}$ kickstage exhaust velocity, m/sec

$\hat{V}_\infty$ direction of outgoing asymptote

ΔV_a apogee delta velocity, m/sec

ΔV_p perigee delta velocity, m/sec

ΔV_T total delta velocity, $\Delta V_T = \Delta V_a + \Delta V_p$, m/sec

u argument of latitude, rad

x,y dummy variables

α angle defined by eq. (B3.4), rad

β mass flow rate, kg/sec

γ adjoint variable associated with thrust direction, kg

δ yaw attitude, rad

ϵ arbitrary constant

ζ dummy variable, sec

η true anomaly, rad

θ defined by eq. (B3.3)

λ adjoint variable associated with velocity, kg-sec^2/m

μ adjoint variable associated with position, kg-sec/m

σ adjoint multiplier associated with mass, sec

τ adjoint variable associated with state variable ζ, kg

φ declination of outgoing asymptote, rad

ψ pitch attitude, rad

Ω longitude of ascending node, rad

$\Delta\Omega$ nodal precession

ω argument of pericenter, rad

$\Delta\omega$ apsidal motion

Subscripts:

D desired

H hardware

i index

Superscripts:

$\bar{}$ vector quantity

$\hat{}$ unit vector quantity

$\dot{}$ time derivative, d/dt

Other notations:

$\cdot$ scalar product of two vector quantities

$\times$ vector product of two vector quantities

$\nabla_{\bar{x}}$ gradient of a scalar with respect to vector x

$|\ |$ magnitude

Δ difference

APPENDIX B

DERIVATION OF EQUATION (21.2)

The gradients of declination with respect to radius and velocity have been derived in reference 1. They are given by

$$\nabla_{\bar{r}}\varphi = \left(- \left[- \tan\alpha\, \hat{r} + \hat{\theta} \right] \cdot \hat{l}_3 \left[\nabla_{\bar{r}}\eta + \frac{1}{e\sqrt{e^2 - 1}} \nabla_{\bar{r}} e \right] + \frac{1}{r} \left[\hat{l}_3 - (\hat{l}_3 \cdot \hat{r})\hat{r} \right] \right.$$

$$+ \tan\alpha \left\{ \left[\frac{2V}{h} (\hat{l}_3 \cdot \hat{V}) - \frac{1}{r} (\hat{l}_3 \cdot \hat{\theta}) \right] \hat{r} \right.$$

$$\left. \left. - \frac{V}{h} \left[(\hat{l}_3 \cdot \hat{r})\hat{V} + (\hat{r} \cdot \hat{V})\hat{l}_3 + \frac{1}{V} (\hat{l}_3 \cdot \hat{\theta}) \nabla_{\bar{r}} h \right] \right\} \right) \frac{\cos\alpha}{\cos\varphi} \qquad \text{(B1)}$$

$$\nabla_{\bar{V}}\varphi = \left(- \left[- \tan\alpha\, \hat{r} + \hat{\theta} \right] \cdot \hat{l}_3 \left[\nabla_{\bar{V}}\eta + \frac{1}{e\sqrt{e^2 - 1}} \nabla_{\bar{V}} e \right] \right.$$

$$\left. + \tan\alpha \left\{ \frac{r}{h} \left[\hat{l}_3 - (\hat{l}_3 \cdot \hat{r})\hat{r} \right] - \frac{\hat{l}_3 \cdot \hat{\theta}}{h} \nabla_{\bar{V}} h \right\} \right) \frac{\cos\alpha}{\cos\varphi} \qquad \text{(B2)}$$

where

$$\sin\varphi = \hat{l}_3 \cdot \hat{V}_\infty \qquad \text{(B3.1)}$$

$$\hat{V}_\infty = \cos\alpha\, \hat{r} + \sin\alpha\, \hat{\theta} \qquad \text{(B3.2)}$$

$$\hat{\theta} = \hat{h} \times \hat{r} \qquad \text{(B3.3)}$$

and

$$\alpha = \cos^{-1} - \frac{1}{e} - \eta \qquad \text{(B3.4)}$$

Adding the cross product of equation (D1) and $\bar{V}$ to the cross product of equation (D2) and $\bar{r}$ gives

$$\nabla_{\bar{V}}\varphi \times \bar{V} + \nabla_{\bar{r}}\varphi \times \bar{r} = \left(-\left[-\tan\alpha\,\hat{r} + \hat{\theta}\right]\cdot \hat{l}\left\{\left[\nabla_{\bar{r}}\eta \times \bar{r} + \nabla_{\bar{V}}\eta \times \bar{V}\right]\right.\right.$$

$$+ \frac{1}{e\sqrt{e^2 - 1}}\left[\nabla_{\bar{r}}e \times \bar{r} + \nabla_{\bar{V}}e \times \bar{V}\right] + \hat{l}_3 \times \hat{r} - \tan\alpha\,\frac{V}{h}\left[(\hat{l}_3 \cdot \hat{r})\hat{V} \times \hat{r} + (\hat{r} \cdot \hat{V})\hat{l}_3 \times \hat{r}\right]$$

$$\left.\left. + \tan\alpha\,\frac{r}{h}\left[\hat{l}_3 \times \bar{V} - (\hat{l}_3 \cdot \hat{r})\hat{r} \times \bar{V}\right] - \tan\alpha\,\frac{\hat{l}_3 \cdot \hat{\theta}}{h}\left[\nabla_{\bar{r}}h \times \bar{r} + \nabla_{\bar{V}}h \times \bar{V}\right]\right\}\right) \frac{\cos\alpha}{\cos\varphi} \tag{B4}$$

It was shown in reference 6, that $\nabla_{\bar{V}}X \times \bar{V} + \nabla_{\bar{r}}X \times \bar{r} = \bar{0}$ if $X = X\left[r, V, \bar{r} \cdot \bar{V}\right]$. In equation (B4) η, e, and h are of this form; therefore, the corresponding cross product sums are zero and equation (B4) reduces to

$$\nabla_{\bar{r}}\varphi \times \bar{r} + \nabla_{\bar{V}}\varphi \times \bar{V} = \left(\hat{l}_3 \times \left\{\tan\alpha\,\frac{rV}{h}\left[\hat{V} - (\hat{r} \cdot \hat{V})\hat{r}\right] + \hat{r}\right\}\right)\frac{\cos\alpha}{\cos\varphi}$$

where the term $rV/h\left[\hat{V} - (\hat{r} \cdot \hat{V})\hat{r}\right] = \hat{\theta}$ and

$$\nabla_{\bar{r}}\varphi \times \bar{r} + \nabla_{\bar{V}}\varphi \times \bar{V} = \frac{1}{\cos\varphi}\,\hat{l}_3 \times \hat{V}_\infty \tag{B5}$$

REFERENCES

1. Barsody, Janos: Three-Dimensional Reusable Tug Trajectories for Planetary Mission Including Correction for Nodal Precession. NASA TN D-8168, 1976.

2. Zimmerman, A. V.: Performance of Recoverable Single and Multiple Space Tugs for Missions beyond Earth Escape. 1972 JANAF Propulsion Meeting. Appl. Phys. Lab., 1972, pp. 627-664.

3. Wolverton, Raymond W.: Flight Performance Handbook for Orbital Operations. John Wiley & Sons, Inc., 1963.

4. Rosendaal, H. L.: A General Branched Trajectory Optimization Algorithm with Applications to Space Shuttle Vehicle Mission Design. AAS Paper 71-326, Am. Astron. Soc., Aug. 1971.

5. McIntyre, J. E.: Guidance, Flight Mechanics, and Trajectory Optimization. Vol. 7: The Pontryagin Maximum Principle. (SID-65-1200-7, Vol. 7, North American Aviation, Inc.; NAS8-11495) NASA CR-1006, 1968.

6. Teren, Fred; and Spurlock, Omer F.: Optimal Three-Dimensional Launch Trajectories with Attitude and Attitude Rate Constraints. NASA TN D-5117, 1969.

7. Spurlock, Omer F.; and Teren, Fred: Optimal Launch Trajectories for the ATS-E Mission. AIAA Paper 70-1051, Aug. 1970.

8. Niehoff, J. C.; and Friedlander, A. L.: Planetary Performance Analysis for Advanced Propulsion Comparisons (APC) Study. Rept. T-33, Sci. Applications, Inc. (NASW-2114), 1972.

TABLE I - NOMINAL MISSION CHARACTERISTICS

Range of vis-viva energy, km^2/sec^2	35 to 120
Range of declinations, deg	-34 to +34
Total trip time, days	1
Tug/kickstage separation coast phase, min	10
Circular departure-orbit altitude, km	185
Departure-orbit inclination, deg	28.5

TABLE II. - BASELINE TUG CHARACTERISTICS

Total vehicle weight, kg	28 622
Weight at Tug burnout, kg	2767
Engine specific impulse, sec	460
Engine thrust, N	66 723
Performance reserve, percent of specific impulse	2
Kickstage adapter weight, kg	45

TABLE III. - KICKSTAGE CHARACTERISTICS

Propellant weight, kg	2306
Specific impulse, sec	378
Stage burnout weight, kg	552
Payload adapter weight, kg	.9
Engine thrust, N	13 345

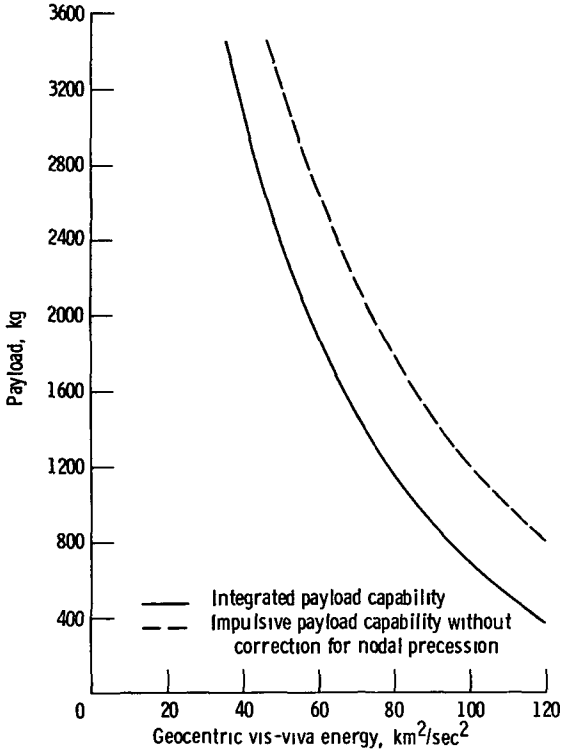

Figure 1. - Effect of mission energy on payload capability of reusable Tug and expendable kickstage for a 0^0 declination.

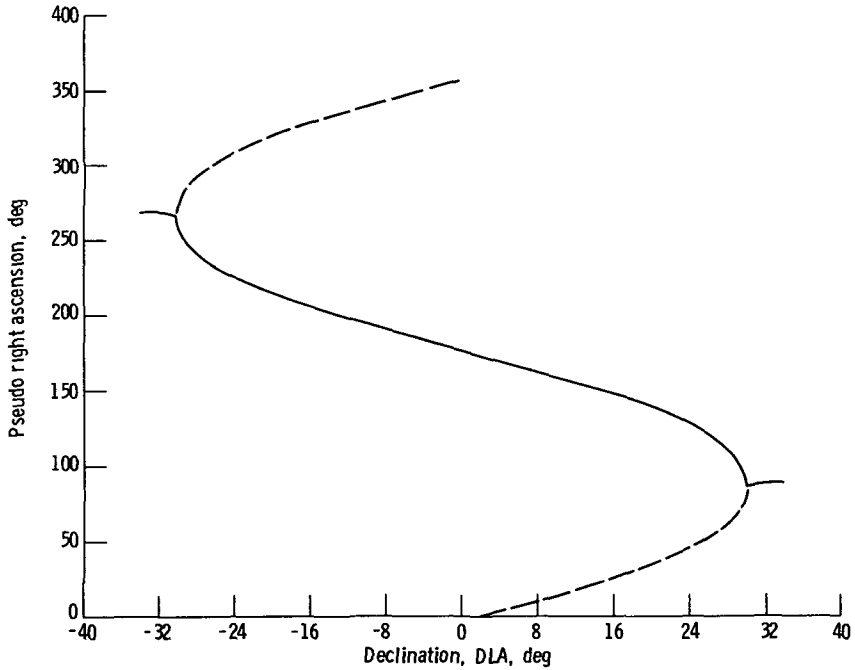

Figure 2. - Optimum pseudo right ascension of the outgoing asymptote measured counterclockwise from Space Shuttle orbit ascending node for a mission energy of 50 km^2/sec^2. Initial SS orbital inclination, 28.5^0

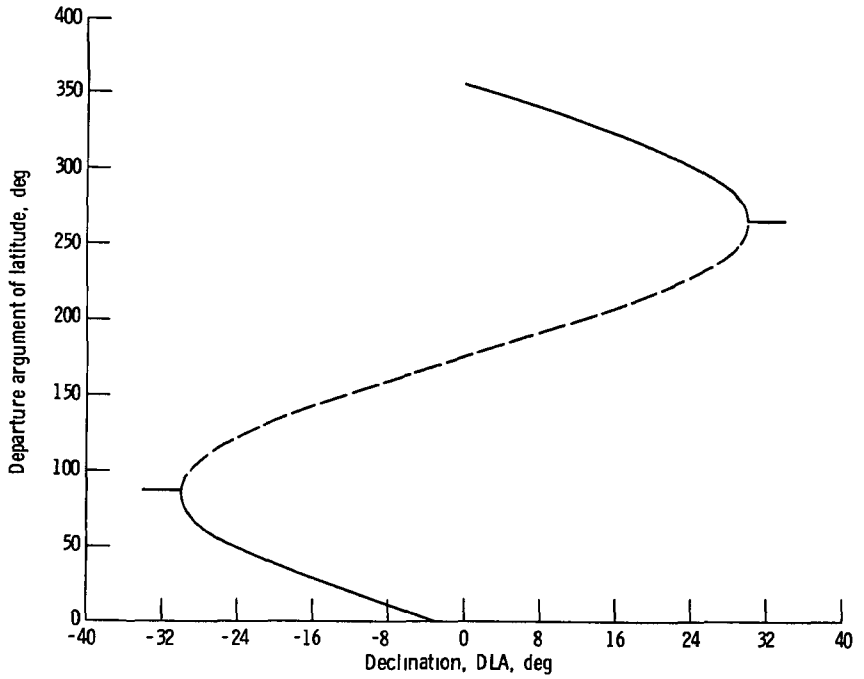

Figure 3. - Optimum Tug departure argument of latitude measured from Space Shuttle orbit ascending node for a mission energy of 50 km^2/sec^2. Initial SS orbital inclination, 28.5^0.

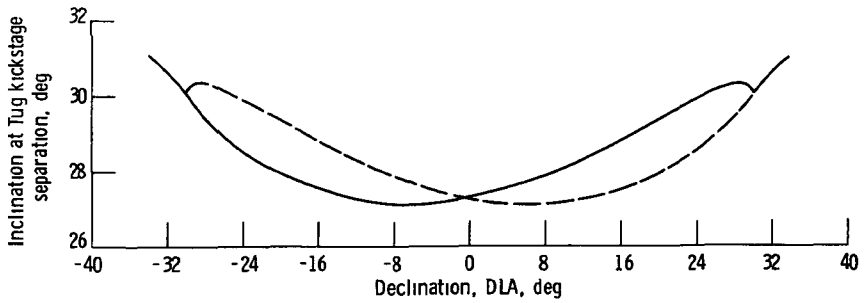

Figure 4. - Hyperbolic orbit inclination at Tug/kickstage separation for a mission energy of 50 km^2/sec^2. Initial Space Shuttle orbital inclination, 28.5^0.

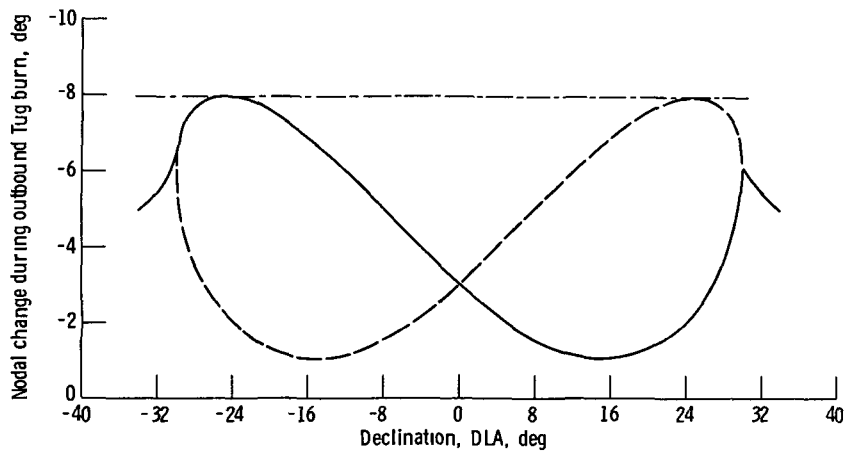

Figure 5 - Correction for Space Shuttle orbit nodal precession during outbound Tug burn for a mission energy of 50 km^2/sec^2 Initial SS orbital inclination, 28 5^0

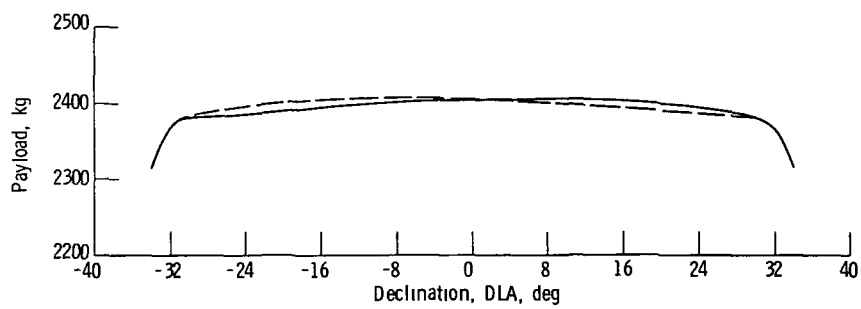

Figure 6 - Optimum payload capability of a reusable Tug/expendable kickstage vehicle for a mission energy of 50 km^2/sec^2 Initial Space Shuttle orbital inclination, 28 5^0

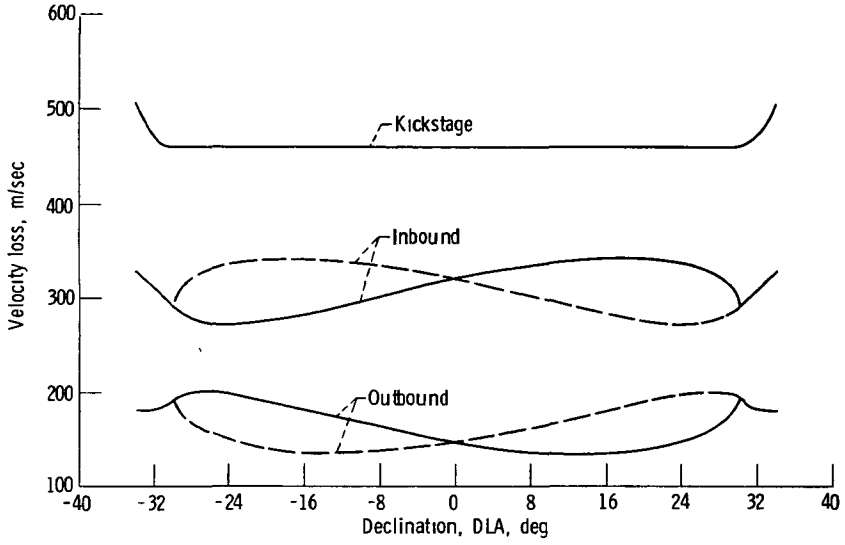

Figure 7 - Velocity loss compared with ideal impulsive orbital transfer for departure from an initial Space Shuttle orbital inclination of 28.5° and a minimum energy of 50 km^2/sec^2

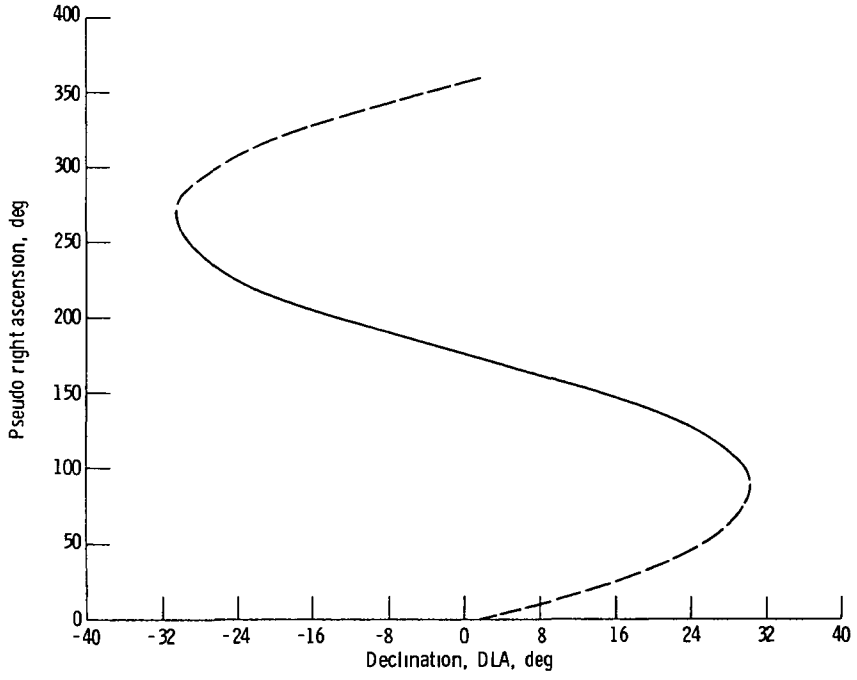

Figure 8. - Optimum pseudo right ascension of the outgoing asymptote measured counterclockwise from Space Shuttle orbit ascending node for a mission energy of 100 km^2/sec^2. Initial SS orbital inclination, 28 5°

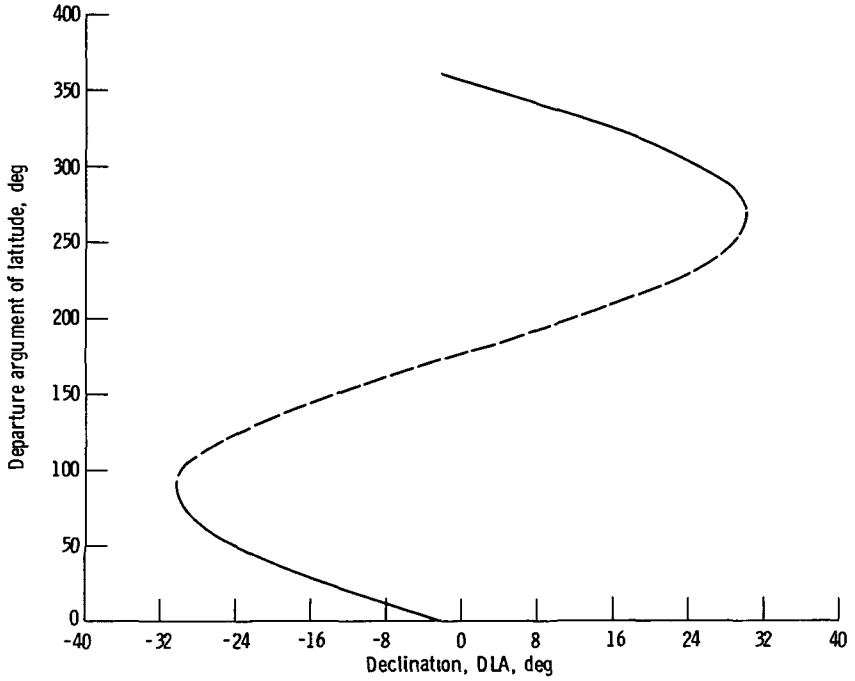

Figure 9. - Optimum departure argument of latitude measured from the Space Shuttle orbit ascending node for a mission energy of 100 km^2/sec^2. Initial SS orbital inclination, 28.5°.

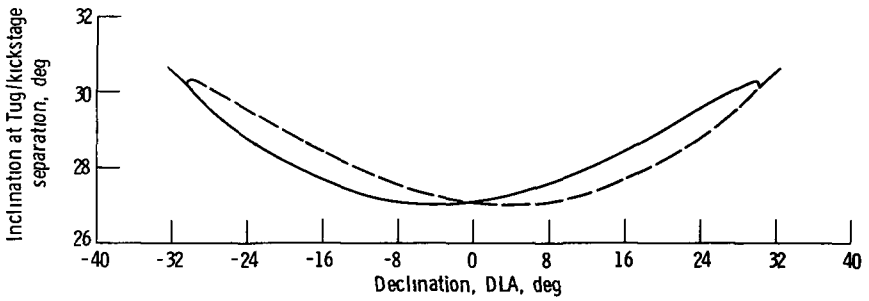

Figure 10. - Hyperbolic orbital inclination at Tug/kickstage separation for a mission energy of 100 km^2/sec^2. Initial Space Shuttle orbital inclination, 28.5°.

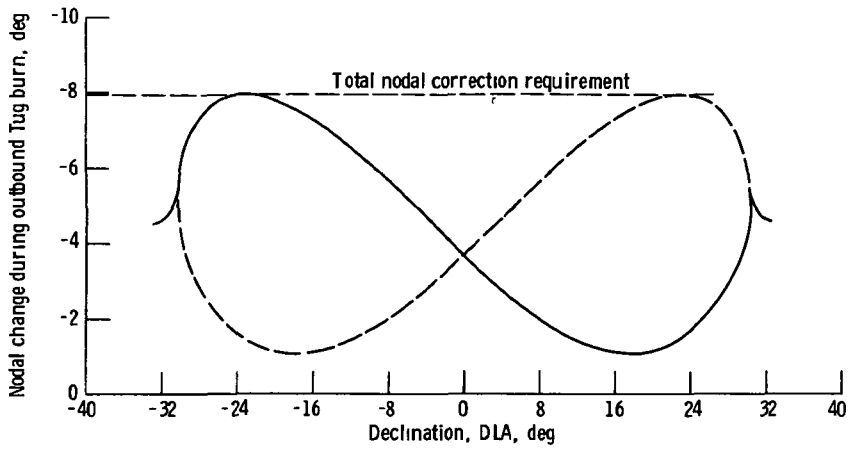

Figure 11. - Correction for Space Shuttle orbit nodal precession during outbound Tug burn for a mission energy of 100 km^2/sec^2. Initial SS orbital inclination, 28.5^0

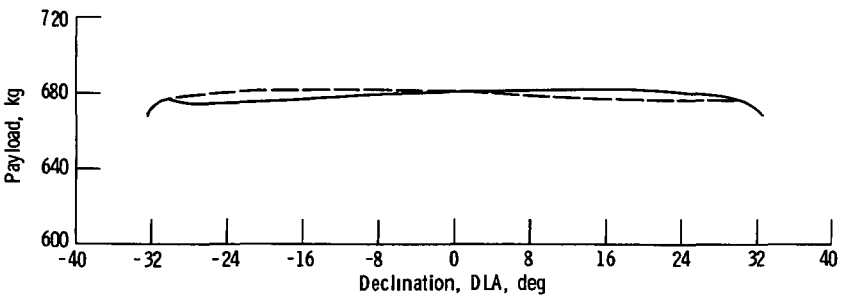

Figure 12 - Optimum payload capability of a reusable Tug/expendable kickstage vehicle for a mission energy of 100 km^2/sec^2. Initial Space Shuttle orbital inclination, 28.5^0.

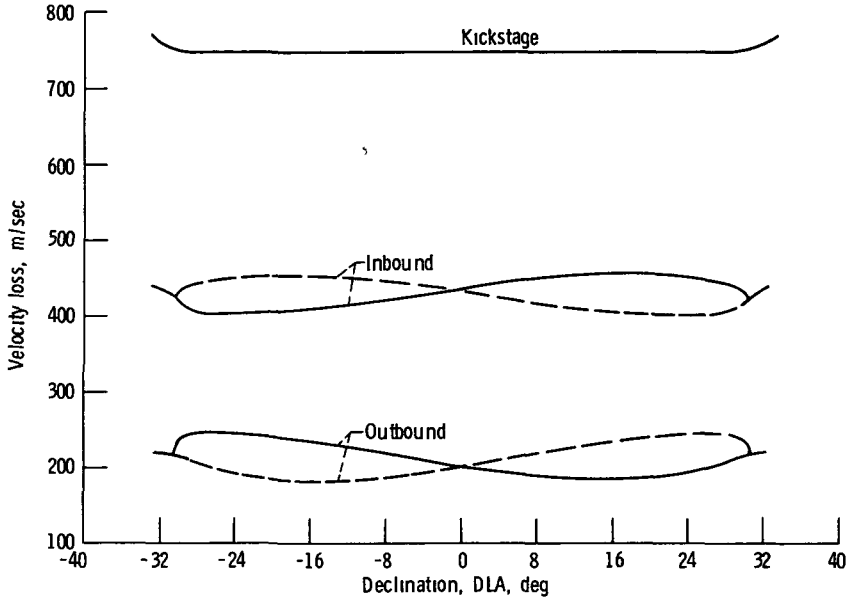

Figure 13. - Velocity loss compared with ideal impulsive orbital transfer for departure from an initial Space Shuttle orbital inclination of 28.5° and a mission energy of 100 km^2/sec^2.

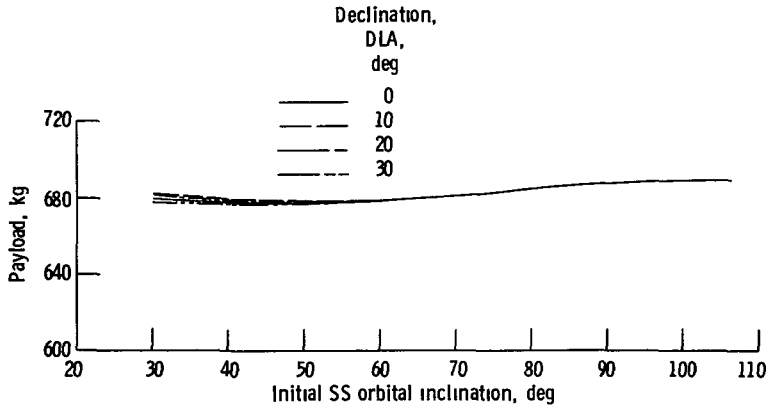

Figure 14. - Effect of initial Space Shuttle orbital inclination on payload.

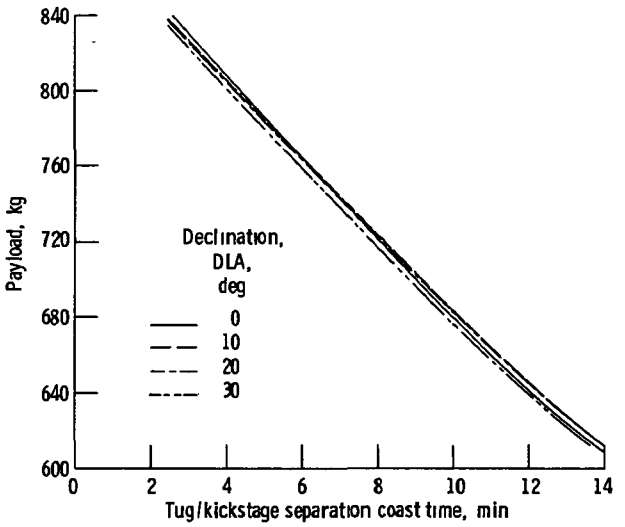

Figure 15. - Effect of Tug/kickstage separation coast time on payload. Initial Space Shuttle orbital inclination, 28.5°; mission energy, 100 km^2/sec^2.

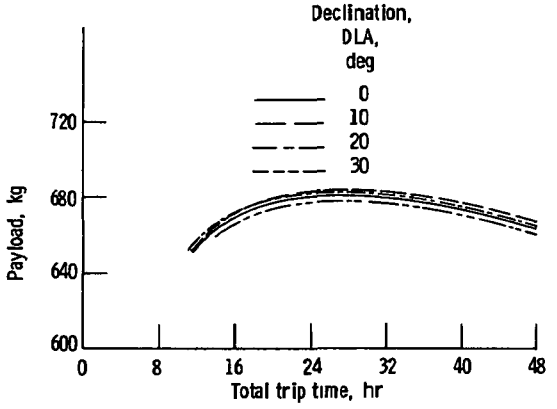

Figure 16. - Effect of Tug total trip time on payload. Initial Space Shuttle orbital inclination, 28.5°; mission energy, 100 km^2/sec^2.

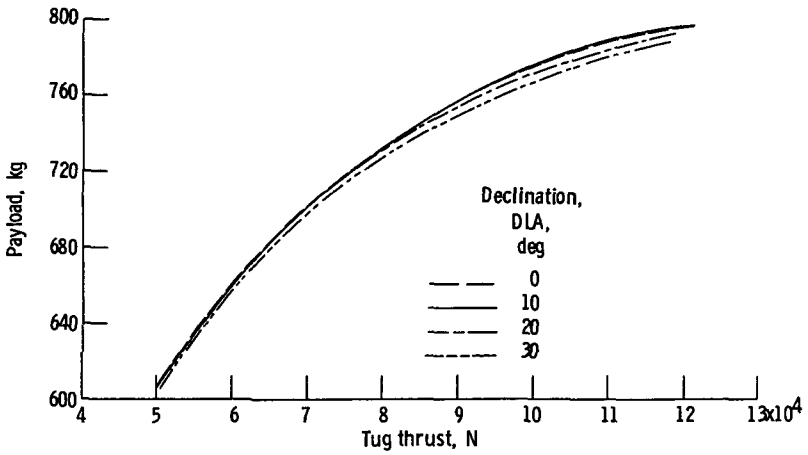

Figure 17. - Effect of Tug initial thrust on payload - fixed Tug engine weight. Initial Space Shuttle orbital inclination, 28.5°; mission energy, 100 km^2/sec^2.

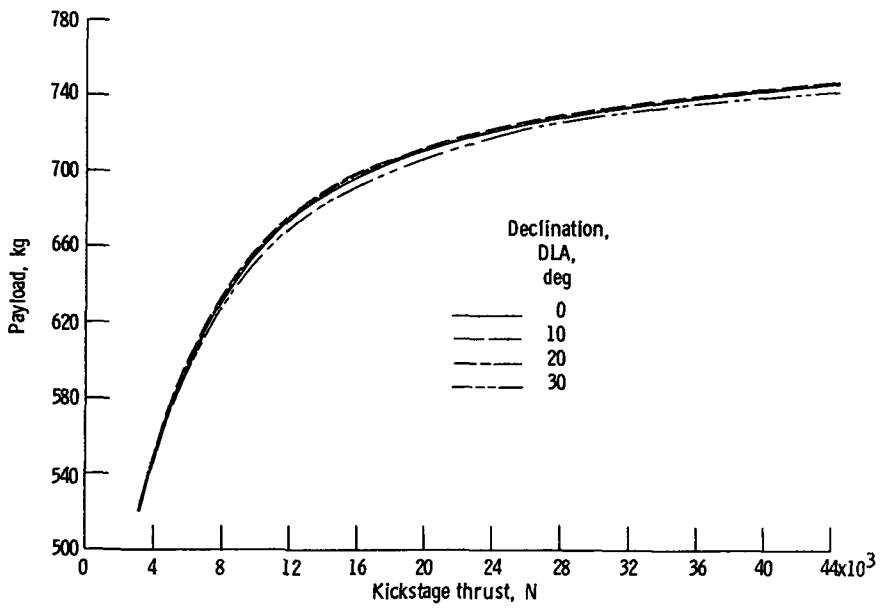

Figure 18. - Effect of kickstage thrust on payload - fixed kickstage engine weight. Initial Space Shuttle orbital inclination, 28.5°; mission energy, 100 km^2/sec^2.

NASA-Langley, 1976 E-8844

"The aeronautical and space activities of the United States shall be conducted so as to contribute . to the expansion of human knowledge of phenomena in the atmosphere and space. The Administration shall provide for the widest practicable and appropriate dissemination of information concerning its activities and the results thereof."

—NATIONAL AERONAUTICS AND SPACE ACT OF 1958

NASA SCIENTIFIC AND TECHNICAL PUBLICATIONS

TECHNICAL REPORTS Scientific and technical information considered important, complete, and a lasting contribution to existing knowledge

TECHNICAL NOTES Information less broad in scope but nevertheless of importance as a contribution to existing knowledge

TECHNICAL MEMORANDUMS Information receiving limited distribution because of preliminary data, security classification, or other reasons Also includes conference proceedings with either limited or unlimited distribution.

CONTRACTOR REPORTS Scientific and technical information generated under a NASA contract or grant and considered an important contribution to existing knowledge

TECHNICAL TRANSLATIONS Information published in a foreign language considered to merit NASA distribution in English

SPECIAL PUBLICATIONS Information derived from or of value to NASA activities Publications include final reports of major projects, monographs, data compilations, handbooks, sourcebooks, and special bibliographies

TECHNOLOGY UTILIZATION PUBLICATIONS Information on technology used by NASA that may be of particular interest in commercial and other non-aerospace applications Publications include Tech Briefs, Technology Utilization Reports and Technology Surveys

Details on the availability of these publications may be obtained from:

SCIENTIFIC AND TECHNICAL INFORMATION OFFICE

NATIONAL AERONAUTICS AND SPACE ADMINISTRATION

Washington, D.C. 20546